Lodders, K., & Fegley, B. (2025). Mineral condensation in stellar outflows. In *Presolar Grains in Extra-Terrestrial Materials: Probing Stars with Stardust* (pp. 539-583). Elsevier. https://doi.org/10.1016/B978-0-12-821830-3.00002-4. Revised 29 August 2024. Preprint.

Mineral Condensation in Stellar Outflows

Katharina Lodders and Bruce Fegley
Department of Earth, Environmental, and Planetary Sciences and McDonnell Center for the Space Sciences, Washington University, Campus Box 1169, One Brookings Drive, Saint Louis MO 63130, USA

Abstract: This article summarizes aspects of the major and trace element equilibrium condensation chemistry of expected minerals forming in circumstellar environments of late type stars (red giant, supernovae, novae). The overall elemental composition is the primary factor controlling the composition of mineral condensates, followed by the density (total pressure and temperature) within the ejecta outflows. For near-solar elemental compositions, mineral condensation sequences are like those computed for a solar composition gas. The carbon-to-oxygen (C/O) ratio governs the redox state of the condensate mineralogy. At C/O from solar to about unity, oxides remain initial condensates with subtle changes for the initially condensing phase and lower condensation temperatures as C/O≈1 is approached. At C/O above unity graphite, carbides, and sulfides are prominent due to the lack of oxygen. Silicates form over a wide range in C/O. Changes in total pressure as well as metallicity also affect the condensate types and their condensation sequences. As presolar grains originated from several generations of different stars the consideration of metallicity is quite important. Starting condensation temperatures for major element minerals and phases as a function of total pressure and metallicity are provided for solar-like elemental compositions which apply to condensation in circumstellar envelopes of red giant and supergiant as well as asymptotic giant branch stars with C/O ratios below unity. The metallicity –dependent chemistry of graphite and carbide condensation at C/O ratios near unity and above is described.

Keywords: presolar grains, condensation temperatures, circumstellar shells, minerals, dust, AGB stars red giant stars, supernovae, stellar winds, thermodynamics, supernova ejecta

Table of Contents

Introduction

Presolar grains found in meteorites formed in the ejecta of evolved stars prior to the formation of the solar system. The stellar sources include red giant branch (RGB) stars, asymptotic giant branch (AGB) stars, supernovae of type Ia (SNIa), novae, mass-losing red (or blue) supergiant (RSG, BSG) and Wolf-Rayet (WR) stars, and supernovae of type II (SNII). The mineralogy and major and trace element compositions of these grains are controlled by the overall elemental composition and the physical conditions such as density, total pressure, and temperature within the stellar ejecta. The stellar ejecta are the best place to probe for nucleosynthesis signatures before the ejecta are diluted with and integrated into matter in the interstellar medium on large spatial and temporal scales.

The application of thermochemical computations to assess which gases and minerals form in stellar environments dates back to pioneering work by Rupert Wildt in 1929 (see review in Lodders & Fegley 1997). Initially, Wildt and other astronomers modified the ionization equilibria (Saha equations) and computed gas phase chemistry without considering condensation of solids. Later work (Wildt 1933) used melting and boiling points, vapor pressure curves, and the Clausius – Clapeyron equation to estimate condensation points for a few refractory materials. Until the late 1940s only limited thermodynamic data for the most common substances were available. The necessity of doing manual computations for systems of coupled-non-linear equations limited quantitative modelling. The development of digital computers and of high-level computer programming languages (e.g. FORTRAN) in the late 1940s and early 1950s revolutionized calculations of simultaneous chemical equilibria in high temperature systems because complex iterative methods became practical. Computational resources tremendously improved since the 1950s and today, complex thermochemical computations can easily be done on laptop

computers. Reviews by Lodders & Fegley (1997), Lodders (2003), and Ebel (2006, 2021) describe the development of thermochemical computations relevant to protoplanetary disks and presolar grains.

The kinds and amounts of dust that can form depend on the total available amounts of the constituent elements, and the condensate stability in the temperature-pressure regime. During cooling of a gas of solar composition, the elements condense sequentially into stable phases determined in part by the particular composition. For solar composition, this gives the cosmochemical classification of the elements as refractory (e.g., Al, Ca, Ti), to intermediate (sometimes also called common or moderately refractory elements such as Mg, Si, Fe), to volatile (P, S, Na, K), to highly volatile (O, C, N, H, noble gases). This is quantified by condensation temperatures, which are temperatures when a phase appears first from the cooling gas, or by 50% condensation temperatures at which half of an element is sequestered into one or more condensates, and the other half remains in one or more species in the gas phase. These condensation temperatures are often the basic underlying concept when elements are described as ”refractory” or “volatile”, or relative volatility trends are discussed in astronomical contexts. This relative volatile/refractory classification scheme also broadly applies to systems of near-solar or solar-like compositions, including metallicity variations (but see below). Many stars and presumably other planetary systems are broadly solar-like in composition and therefore the use of this volatility classification of the elements derived from solar composition is widely applicable.

One major application of condensation models is to understand the composition of dust formed in different astronomical environments as a function of pressure, temperature, and metallicity. For example, it is convenient to describe depletions of elements relative to solar composition within a gas such as the interstellar medium by the removal of refractory elements into condensate dust, or to ascribe the relative depletion of volatile elements in meteorites to incomplete condensation. This works well as long as solar composition is the baseline for both – the measure of the relative depletions or enrichments by normalizing to solar composition, and of the volatility (or condensation) sequence as calculated for a solar composition gas.

Many of the known presolar grains must have formed in environments that are considerably non-solar in composition and their mineralogy (e.g., SiC, graphite, Si_3N_4) is neither expected nor stable in solar composition gas. Known stellar sources such as carbon stars, supernovae, and novae are characterized by non-solar elemental compositions, so the chemistry is different. Therefore, the variations in elemental abundances measured in presolar grains relative to solar can stem from both, chemical elemental fractionations during condensation as well as changes to the presumed initially solar-like elemental abundances by nucleosynthetic contributions during evolution of the grains’ parent stars.

Elemental Compositions

Many calculations have been done for modelling dust condensation and stability in a gas of solar composition, and results from such calculations have found wide applications in astronomy and cosmochemistry (e.g., see Lodders 2003, 2020, Ebel 2006, 2021 and references therein). The use of solar elemental abundances was motivated by the desire to understand how the primordial solar-system elemental abundance mixture that is still recorded in the Sun’s composition now would lead to the element fractionations that gave rise to the chemical plentitude seen in the planets, their natural satellites, asteroids, Kuiper-Belt objects, and comets.

Lodders, K., & Fegley, B. (2025). Mineral condensation in stellar outflows. In *Presolar Grains in Extra-Terrestrial Materials: Probing Stars with Stardust* (pp. 539-583). Elsevier. https://doi.org/10.1016/B978-0-12-821830-3.00002-4. Revised 29 August 2024. Preprint.

Many dwarf stars like our sun have similar heavy element ratios for elements heavier than helium, e.g., such as Mg/Si, Al/Si, or Fe/Si; however, there could be variations in the ratios of heavy elements relative to hydrogen (i.e., metallicity). Like other stellar systems with and without planets, the solar system likewise formed from gas and dust of an interstellar molecular cloud. The gas (mainly H and He) within the interstellar medium is still largely of primordial origin, whereas heavier elements were and are built by nucleosynthesis processes in multiple generations of stars and released over time into the interstellar medium when stars end their lives. To first order, the ratio of heavy elements relative to hydrogen (the metallicity) increases regularly over time.

Main-sequence stars like the sun and with metallicities ranging from about 0.03 – 3 times solar have more oxygen than carbon, and C/O ratios of around 0.5. Dwarf stars within the solar mass range only have small mass loss rates (e.g., the sun loses about 10^{-14} of its mass per year) and there is usually no circumstellar environment that allows grain formation. On the main sequence of stars in the Hertzsprung-Russell diagram dwarf stars burn H to He in their cores and after H fuel exhaustion, H-core burning ends. Stars evolve off the main sequence onto the giant branch(es). All heavy element nucleosynthesis, and therefore the base composition for circumstellar grain formation, essentially happens after stars leave the main sequence.

The initial mass of a star controls its lifetime during its different stages of evolution as well as its evolutionary path off the main sequence, the nucleosynthesis processes, and final overall elemental composition of a star. Usually, the grouping is low mass stars with 1.3- 3.5 $M_{\odot}$, intermediate mass stars with 3.5-9 $M_{\odot}$, and massive stars above 9 $M_{\odot}$. Two cases are distinguished: low- and intermediate mass stars (final stages towards RGB, AGB), and massive stars (final stages towards SNII). Initial stellar mass also determines how and how much of a star's mass is returned to the interstellar medium at the end: Either through stellar winds in low and intermediate mass RGB, AGB stars, or for massive stars through strong winds (RSG, WR) followed by violent core-collapse SN explosions (SNII).

The increase in heavy elemental abundances over time is the topic of Galactic chemical evolution. Integrated over time, the interstellar medium received about solar relative proportions of the heavy elements from several generation of stars. Star formation for a given stellar generation leads to a similar range of initial stellar masses (called the initial mass-function). The time-integrated release of the different nucleosynthesis products from low- and intermediate mass stars (evolving to AGB stars and leaving white dwarfs as remnants) plus massive stars (evolving to SNII and leaving neutron stars or black holes as remnants) leads to about constant relative proportions of heavy elements. The situation was somewhat different for the formation of the earliest low metallicity stars (<< 0.03 the solar heavy element content) because longer stellar lifetimes of low and intermediate mass stars caused a delay in release of AGB star products, and the release of Fe-peak elements from SN Ia, which occur after mass transfer onto white dwarfs causes complete disruption of the AGB remnant.

Because of the similarities in stellar evolution over time, the resulting elemental compositions and the dust resulting from the stellar ejecta as functions of initial stellar mass will be similar. This explains the correlations seen in the chemical and isotopic compositions in different types of presolar grains although they originated from many stars of similar types.

Lodders, K., & Fegley, B. (2025). Mineral condensation in stellar outflows. In *Presolar Grains in Extra-Terrestrial Materials: Probing Stars with Stardust* (pp. 539-583). Elsevier. https://doi.org/10.1016/B978-0-12-821830-3.00002-4. Revised 29 August 2024. Preprint.

Ejecta of Low- and Intermediate Mass Stars

Red giants and AGB stars are late type, low mass (1.3 -3.5 $M_\odot$) to intermediate mass stars (3.5 -9 $M_\odot$). On the red giant branch some mass loss can occur but stellar mass loss becomes pronounced and fast when these stars move onto the asymptotic giant branch (AGB). All that will remain are the CO-rich or ONeMg-rich cores of former AGB stars, which become white dwarfs with about 0.6-0.9 $M_\odot$, and Earth-size diameters. The mass-loss from an AGB star proceeds from the outer layers by stellar winds into huge circumstellar envelopes (CSE) within about 1-3 million years, and it is at this stage that grain formation proceeds. During the subsequent post-AGB and planetary nebula phase the CSE has expanded farther into the ISM and becomes UV photoionized by radiation from the remaining hot white dwarf; the possible processes operating on grains (photoevaporation, sputtering) and potential chemical and isotopic effects are not well understood and require more studies.

Changes of elemental abundances relative to solar during the late evolution of low and intermediate mass stars is well documented by stellar spectroscopy and understood from nucleosynthetic computations. The chemical changes in the outer regions during the giant star phase are indicated in the following scheme shown in Figure 1 where we assume that a star initially had solar composition:

Red Giant Branch RGB C/O ≤ 0.5(solar)	*Asymptotic Giant Branch, AGB M stars C/O ≈ 0.5(solar)-0.9*	*Asymptotic Giant Branch, AGB S stars C/O ≈ 0.9-1*	*Asymptotic Giant Branch, AGB C stars C/O > 1*
Sum C+N+O≈ solar *C ≤ solar* *N ≈ 1 - 10x solar* *O ≥ solar* *Increased over solar:* *^{13}C, ^{14}N, ^{17}O* *Solar s-process elemental abundances*	*C ≳ solar and C < O* *N ≈ 10x solar* *O = solar* *Increased over solar* *^{12}C, ^{13}C, ^{14}N, ^{17}O* *s-process element ≥ solar*	*C ≈ O* *N ≈ 10x solar* *O = solar* *Increased over solar* *^{12}C, ^{13}C, ^{14}N, ^{17}O* *s-process elements > solar*	*C > O* *N≈10x solar* *O = solar* *Increased over solar* *^{12}C, ^{13}C, ^{14}N, ^{17}O* *s-process elements > solar*

Figure 1: A summary of chemical changes in the outer regions of giant stars (RGB, AGB).

We only briefly mention here the fates of white dwarfs (the AGB remnants) as they also may turn into dust producers. A white dwarf in a binary (or multiple) system may receive mass transfer from a companion star. Depending on the orbital separation of the binaries and mass transfer rates, the result is either a nova or a supernova type Ia explosion. Slow accretion rates may cause ignition of H-burning in the accreted matter on the surfaces of white dwarfs, leading to recuring nova events. Novae are relatively rare, and their elemental compositions are H-poor and either C + O, or O +Ne dominated. During nova nucleosyntheses, elemental and isotopic compositions up to sulfur are affected; in ONe novae this may go up to Ca (e.g., Jose et al. 2004, Jose and Hernanz 2007). The elemental composition of the ejecta have been observed to be either O or C rich, leading to oxidized or reduced (C-rich) condensates. There are clear indications that oxidized and reduced material is mixed, leading to co-condensation of both carbonaceous and silicate dust in nova outflows (Haenecour et al. 2019**)**. Nucleosynthesis and condensation modelling in nova ejecta with applications to presolar grains is given by e.g., Jose et al. 2004, Haenecour et al. 2016, 2019.

Lodders, K., & Fegley, B. (2025). Mineral condensation in stellar outflows. In *Presolar Grains in Extra-Terrestrial Materials: Probing Stars with Stardust* (pp. 539-583). Elsevier. https://doi.org/10.1016/B978-0-12-821830-3.00002-4. Revised 29 August 2024. Preprint.

Supernovae of type Ia occur when large mass transfer rates or binary mergers increase the mass of a white dwarf towards or above the Chandrasekhar limit of about 1.44 $M_{\odot}$. Once temperatures and pressures become high enough, carbon fusion ignites and subsequent runaway fusion of O and Si leads to a type Ia supernova explosion that disintegrates the star. Nucleosynthesis in SNIa provides large yields in iron peak elements (Cr, Mn Fe, Co, Ni, Cu, Zn; among them neutron-rich nuclides such as ^{54}Cr, ^{50}Ti, ^{58}Fe, and ^{62}Ni (Nomoto et al. 1997, Lach et al. 2020)). Hydrogen and He are essentially absent; C, O and Ne abundances in the ejecta may depend on how much of the outer white dwarf layers escape nuclear processing. Overall, other lighter elements such as Mg, Si etc. are present but their yields depend on the details of the binary companion, the physics of the mass transfer or merger; the densities and temperatures reached before explosion, and the thermonuclear explosion mechanisms.

Detailed modelling of grain formation in type SNIa to predict the potential dust mineralogy has not been done. The gas and condensate chemistry of type Ia supernovae will be completely different than for H and He rich solar-like compositions. There are only very few presolar grains known that came from SNIa, probably including Cr-rich spinel, but these spinels could also come from rare electron-capture supernovae (Nittler et al. 2018, Hoppe et al. 2022).

Abundances of overall ejecta for SNIa from Carbon-Oxygen-rich white dwarfs (CO WD) by Woosley (1997) give C/O from 0.005 to 3 (most around 1.2; solar = 0.5), depending on model parameters, and Si/O ratios ranging from 0.05 to 0.5 (with extreme cases around 5300). The enrichment of Fe-peak elements is evident from Fe/Si ratios ranging from 6 to 170, the solar ratio is 0.9. More confined ejecta zones will have more extreme compositions. As long as there is some C, N, and O, oxides, nitrides, and carbides might form. The sulfur chemistry could become important, and sulfides as well as silicides may form. From previous work on SN II ejecta modelling (Lodders 2006) and novae (Jose et al. 2004, Haenecour et al. 2019) for presolar grains we may also expect other exotic compounds such as titanides.

Red Giant Branch (RGB) Stars

Helium production through core H chain burning dominates in less massive dwarf stars such as the sun whereas in stars above 1.5 $M_{\odot}$ the H in their cores burns via the catalytic CNO cycle (see e.g., Wiescher et al. 2010). After H core burning, stars make their first ascent to the red giant branch in the Hertzsprung-Russell diagram. They burn H to He in a shell around their inert He-rich cores. A byproduct of CNO-burning is nitrogen at the expense of carbon and oxygen. Depending on which of the four different CNO cycles is active, the sum of CNO nuclei remains more or less constant but ^{14}N, ^{13}C, ^{17}O are increased; and the production of F might also be possible (see Wiescher et al. 2010, Abia et al. 2017). The expanded star has a convective outer shell and the byproducts of H-burning via the CNO cycle are mixed to the stellar surface. This is the “first dredge-up” and the reason why red giants show enhanced nitrogen abundances relative to solar, and somewhat decreased O and C abundances. Overall, the increase in N abundance up to a factor of 10 above solar and the slight decrease in C/O below solar are the most important changes that affect the chemical speciation and condensation temperatures of potential condensates from red giant branch stars when compared to solar composition. Once H-shell burning has increased the mass of He in the core, helium core burning sets in and the RGB phase ends; the star may move to the horizontal branch. The products of He-core burning are mainly ^{12}C and ^{16}O, which remain as the main constituents of the inert core once He-core burning ends.

Lodders, K., & Fegley, B. (2025). Mineral condensation in stellar outflows. In *Presolar Grains in Extra-Terrestrial Materials: Probing Stars with Stardust* (pp. 539-583). Elsevier. https://doi.org/10.1016/B978-0-12-821830-3.00002-4. Revised 29 August 2024. Preprint.

Asymptotic Giant Branch (AGB) Stars

After the RGB and subsequent He-core burning, nucleosynthesis proceeds with alternating H- and He burning in shells surrounding an inert CO core. The star ascends on the asymptotic giant branch (AGB). The recurring ignition of He burning every 1,000- 10,000 years in shells around the core is called a "thermal pulse" (not to be confused with the variability pulsation cycle of the outer star with periods of around a year which is important for grain formation and mass loss from the star, see below).

The major change in composition is the addition of ^{12}C from triple alpha-burning to the outer convective envelope of the star. This causes the increase in the C/O ratio. However, in more massive stars also some oxygen (^{16}O) is made. During He-shell burning, slow neutron capture nucleosynthesis (the *s*-process) is activated (see chapter by Lugaro et al., this volume, and e.g., review by Herwig 2013). The *s*-process raises the elemental abundances for heavy elements beyond the Fe-peak and affects elements largely comprised of isotopes made by the *s*-process, such as Y, Zr, Sr, Ba, Mo, Tc, Ru, Pb, and some of the rare earth elements (REE, also called lanthanides).

Associated with the multiple thermal pulses are "third dredge ups" where ^{12}C (and possibly ^{16}O) from He-shell burning and the *s*-process elements are mixed up to the stellar surface by convection. At the same time, mass-loss from the star (around 10^{-5} to 10^{-7} $M_\odot$ per year) controls how long the star can remain in the ABG burning configuration which in turn determines how much carbon is made that can be mixed up. The typical mass loss rates of 10^{-5} to 10^{-7} $M_\odot$ per year limit the lifetime of the AGB stage to a few million years depending on initial mass; e.g., an initially 3.5 solar $M_\odot$ star converting to a 0.5 $M_\odot$ white dwarf will lose 3 $M_\odot$ within 3 million years at $dM/dt = 10^{-6}$ $M_\odot$/year.

It is thought that only stars with initial masses around 1.3 – 3.5 solar masses can reach C/O ratios above unity and become carbon stars. Intermediate mass stars (initially with about 3.5-8 $M_\odot$) remain O-rich because of hot-bottom burning (see chapter by Lugaro et al., this volume). At lower metallicities somewhat more massive stars can also become carbon stars because the absolute initial amounts of oxygen are lower and less freshly produced carbon is needed to raise the C/O ratio. However, mass loss also decreases the stellar mass and at some point, the mass of an initially intermediate mass star will have decreased to 1-3 $M_\odot$ on the way to becoming a WD. Then HBB stops and the star still can become a C star (see Frost et al. 1998).

The gradual change in C/O during stellar evolution on the AGB will also lead to a gradual change in C/O in the wind that is released and can cause time and location dependent compositional variations within the CSE structure. Thus, the innermost regions of the envelope can have elevated C/O over the outmost regions where compositions are closer to the solar C/O ratio. This gradation in C/O should influence observable grain compositions which parallels the C/O ratios: Reduced carbonaceous dust closer to the star and more oxidized gas and dust species at the outer edges of the circumstellar envelope. However, the chemical gradation could be difficult to discern as mass loss rates are not necessarily constant and also depend on the amounts of dust present because radiation pressure on grains drives mass loss and wind acceleration to terminal velocities around 15-25 km/s in CSEs. Thus, it is a balance of timing for reaching high C/O through third dredge ups and release into the CSE, the size of the envelope, and expansion velocities for having oxidized and carbonaceous dust present within the same CSE. Oxidized

grains could be lost to the ISM long before carbonaceous dust has reached similar distances within the CSE, and not much is known about how well gas and dust could be mixed over large scales.

Condensation Calculations

General Considerations for Condensation Computations

Ideal gas chemical equilibrium (aka thermochemical equilibrium) computations require as input the temperature, total pressure, temperature dependent standard Gibbs free energies of formation ($\Delta_f G°$) for each species, and the bulk elemental composition of the system to uniquely describe the distribution of elements among all gas and condensed phase species. Thermodynamic data compilations such as the NIST-JANAF Tables (gases and some minerals), and the US Geological Survey compilation by Robie and Hemingway (1995) for minerals are widely used sources of $\Delta_f G°$ values used in ideal gas chemical equilibrium calculations. Fegley et al. (2023) noted the IVTAN database (Belov et al. 1999), which is the Russian counterpart to the NIST-JANAF Tables, is being continually updated and covers a wider range of elements and compounds than the NIST-JANAF Tables. As noted elsewhere (e.g., Lodders 1999, 2004, Ruscic et al. 2002) there are errors in the NIST-JANAF Tables that must be considered, or else incorrect input values are used in calculations. A similar problem exists with some of the fit coefficients of Sharp and Huebner (1990) that lead to erroneous results as shown elsewhere (Lodders 2002).

Gases behave ideally at the low total pressures encountered in CSE and stellar photospheres and real gas corrections are unnecessary. This is easily shown using the virial equation of state (e.g., Hirschfelder et al. 1964). Formation of mineral solid solutions, e.g., melilite at C/O = solar may require activity coefficients for the solid solution components unless ideality is assumed. However even if mineral solid solutions are non-ideal, ideality is a good approximation unless activity coefficients deviate from unity by large amounts (e.g., see discussion in Fegley et al (2023) for oxide melts).

We use condensation of titanium carbide TiC in the circumstellar envelope of a carbon star to illustrate a chemical equilibrium computation. The total abundance of the element Ti in all forms is A_{Ti}, which is the input elemental abundance used in the calculations. Depending upon the stellar abundance model used, A_{Ti} could be less than, equal to, or greater than the Ti solar elemental abundance. The total mole fraction X of the element Ti is the ratio of A_{Ti} to the abundances of all other species,

$$X_{\Sigma Ti} = \frac{A_{Ti}}{\left(A_H + A_{H_2} + A_{He} + \cdots\right)}$$

The sum in the denominator includes the temperature dependent atomization of H_2 and all other species in the computations, such as CO, C_2H_2, N_2, etc. which are omitted here for clarity. The total pressure of the element Ti in all forms equals the sum of partial pressures of Ti-bearing gases, e.g.,

$$P_{\Sigma Ti} = X_{\Sigma Ti} P_{Total} = P_{Ti} + P_{TiO} + P_{TiO_2} + P_{TiS} + P_{TiF} + P_{TiC_2} + \cdots$$

The actual mass balance sum used in the CONDOR code contains 31 Ti-bearing gases and also includes thermal ionization (e.g., Ti^+, Ti^{+2}, Ti^-, TiO^+). The mass balance equation is rewritten in terms of the thermodynamic activity of Ti (a_{Ti}), the equilibrium constant for forming a gas from its constituent elements in their reference states (K_{gas}), and the activities (a_{gr} for graphite) or fugacities (f_E for E = O_2, S_2, F_2, etc.) of the other elements combined with Ti in the gas, e.g.,

$$P_{\Sigma Ti} = a_{Ti}\left[K_{Ti} + K_{TiO}f_{O_2}^{1/2} + K_{TiO_2}f_{O_2} + K_{TiS}f_{S_2}^{1/2} + K_{TiF}f_{F_2}^{1/2} + K_{TiC_2}a_{gr}^2 + \cdots\right]$$

The most important term in the titanium mass balance sum is the partial pressure of monatomic Ti gas, which is about 10^5 times larger than the partial pressure of any other Ti-bearing gas. Titanium oxide gases are insignificant while they are major species in a solar composition gas.

Each element included in the calculations has an analogous form of the titanium mass balance sum. The gases included in the calculations are listed elsewhere (e.g., Fegley and Lodders 1994, Lodders and Fegley 1993, 1995). The necessary equilibrium constants are from JANAF or IVTAN. Unlike chemical kinetic codes, chemical equilibrium calculations do not involve any guesswork about reaction networks. This is completely unnecessary because thermodynamic functions such as internal energy U, enthalpy H, entropy S, Gibbs energy G, and Helmholtz energy A are perfect differentials, i.e., thermodynamic calculations are path independent (e.g., see Fegley 2013).

The coupled nonlinear mass balance equations are solved iteratively using a computer program such as the CONDOR code (Lodders and Fegley 1993). The initial guess for the activity (or fugacity) of each element can be unity or it can be optimized using some knowledge of the system's chemistry, e.g., all C as C_2H_2, all O as CO, all N as N_2, all metals as monatomic gases, and so on. The code solves the mass balance equations and gives the chemical equilibrium abundances of all species (atoms, ions, molecules, and radicals) included in the input database. A solution is reached when mass balance is reached, i.e., the absolute value of the input and calculated elemental abundances agree within a certain criterion,

$$\left|\left(\frac{output}{input} - 1\right)\right| \ll 10^{-9}$$

It may sound trivial, but surprisingly in some codes mass-balance is not enforced. This should be carefully evaluated when computational results are used to interpret observational data such as gas species abundances in circumstellar environments or in presolar grains.

Once gas phase chemistry is solved, condensate stability is computed using compound formation from the elements in their respective reference states, e.g.,

Ti (ref) + C (graphite) = TiC (titanium carbide)

The equilibrium constant expression for the formation of TiC is

$$K_{TiC} = \frac{a_{TiC}}{a_{Ti(ref)}a_{gr}}$$

The code gives the activity of graphite and the activity of Ti, whose reference state varies from metal to liquid to gas with the transitions occurring at the melting point and the normal boiling point (of course either coexisting phase is a valid reference state at the transition points).

Titanium carbide condenses at a temperature where its thermodynamic activity equals unity and this is calculated by rearranging the equilibrium constant expression:

$$a_{TiC} = K_{TiC}a_{Ti(ref)}a_{gr}$$

Note that no assumptions whatsoever about any reaction networks are needed for this calculation.

Once TiC is stable and its activity is fixed at unity, the fraction of Ti in TiC, denoted α(Ti), is computed and the gas phase abundance of Ti ($P_{\Sigma Ti}$) is reduced by multiplying by [1 – α(Ti)]. Analogous corrections are made for C when graphite condenses, for Si when SiC condenses and so on. The gas phase and gas solid chemical equilibrium calculations are done simultaneously using iterative methods. More detailed descriptions of the CONDOR code chemical equilibrium calculations are given elsewhere (Lodders and Fegley 1993, Fegley and Lodders 1994, Lodders 2003).

Thermochemical equilibrium means that for a system at constant temperature and total pressure, a state of energetic minimum (Gibbs free energy minimization) between all (gas and condensate) reactions is reached. This does not mean that all reactions have stopped - reactions are still ongoing in the thermochemical equilibrium state, but forward (e.g., formation) and backward (e.g., destruction) reactions proceed at the same rates (steady state). In this context we caution that steady state alone is not a sufficient criterium for equilibrium because steady state is also reachable for so-called local equilibria which are close to but not at energetic minimum.

Many codes use Gibbs-Energy minimization routines which solve for the distribution of the elements into different gaseous and condensed compounds that results in the lowest energy state of the overall system. Computational problems can arise if codes run into “local minima” (potential meta-stable states) or if the stability of too many potential condensed phases must be sorted through. The clear advantage of equilibrium thermodynamics is that the results are path-independent of the actual elementary reactions occurring in a system, and that the results for net reactions are obtained. At equilibrium, formation and destruction reactions still occur in a system, but are at balance, hence equilibrium. The disadvantage is that equilibrium thermodynamics does not describe how quickly an equilibrium state is reached, or which reaction steps for the formation of each gaseous compound or condensate are actually happening. Equilibrium computations are good models of chemistry at high temperatures and “high” total pressures (e.g., relative to those in the ISM).

For example, Symonds et al (1994) demonstrate that chemical equilibrium calculations are valid for terrestrial volcanic gases down to 500 °C ($P_{Total} \approx 1$ bar). Aller (1963) shows ionization equilibria in stellar photospheres correctly predict the observed ionization states of elements at high temperatures and total pressures $\gtrsim 10^{-7}$ bar. Palme and Wlotzka (1976) and Blander et al (1980) showed the measured composition of refractory metal (Os, Re, W, Mo, Ir, Ru) nuggets in Ca, Al – rich inclusions in Allende matches the calculated composition at high temperatures (>1600 K) and low total pressures 10^{-3} – 10^{-4} bar where the CAIs are calculated to have formed from solar nebula gas (e.g., see the review by Grossman 1980). However, we need to keep in mind that the temperature and pressure conditions for equilibrium may vary for each element and its compounds because different elementary reactions that can be rate limiting steps are quenched (or frozen in) at different temperatures and densities. We return to this point in the next section.

It is important in all computational approaches that as many elements and compounds as possible are included for the simple reason if a compound is not considered, its importance for the overall chemistry in a system would be ignored. In practice, the major element gases and condensates at C/O ratios ≥solar are known. For example, at high temperatures where grains form, the major gases of carbon and oxygen at different C/O ratios are CO plus either H_2O or C_2H_2 (the latter two being far more reactive than CO).

These gases (plus H_2) determine the redox state and speciation of the gases and condensates of other less abundant elements (e.g., SiO (g) and silicates for C/O < 1 and Si (g), SiC_2(g) and SiC (s) for C/O >1).

Kinetic Effects

A quantitative discussion of kinetic effects and deviations from equilibrium first requires knowledge of equilibrium compositions, which are computed as described above. At high temperatures in the inner regions of CSE exothermic reactions will be rapid with bimolecular rate constants reaching 10^{-10} – 10^{-9} cm^3s^{-1}, i.e., the gas kinetic rate. Endothermic reactions will proceed slower and have activation energies at least as large as reaction endothermicity. Reaction rate constants are better known for metal – metal oxide – metal hydroxide chemistry applicable to C/O <1 environments but generally must be estimated for reactions of interest in reducing stellar atmospheres. Unimolecular and bimolecular reactions are expected to be more important than termolecular reactions because of the low number densities in stellar atmospheres. Following past work in the planetary literature (e.g., Prinn and Barshay 1977, Fegley and Prinn 1985, Prinn and Fegley 1989, Fegley and Lodders 1994), it is convenient to define t_{chem} as the thermochemical reaction time, and t_{cool}, as the physical cooling time given respectively by

$$t_{chem} = -\left(\frac{dln[i]}{dt}\right)^{-1}$$

$$t_{cool} = -\left(\frac{dlnT}{dt}\right)^{-1}$$

Where t is time (s), [i] is the number density of species i (particles cm^{-3}), and T is absolute temperature (K). In the hotter, denser, inner regions of a CSE, chemical equilibrium is reached because,

$$t_{chem} < t_{cool}.$$

Conversely, chemical equilibrium is not reached in the cooler, lower density, outer regions where,

$$t_{chem} > t_{cool}.$$

Chemical equilibrium is frozen in, or quenched, in an intermediate region of a CSE where,

$$t_{chem} = t_{cool}.$$

Thermochemical reactions with chemical reaction rates R given by an Arrhenius expression (with E_A activation energy, N_A Avogadro's number and k_B Boltzmann's constant),

$$R \propto exp\left(\frac{-E_A}{N_A k_B T}\right)$$

ultimately are kinetically inhibited as temperature decreases because the chemical deceleration time t_{decel} is smaller than the cooling time:

$$t_{decel} = -\left(\frac{dlnR}{dt}\right)^{-1} = \left(\frac{N_A k_B T}{E_A}\right) t_{cool} \ll t_{cool}$$

With constant cooling time, thermochemical reactions with smaller activation energies will maintain equilibrium within a larger region in a CSE, than will reactions with larger activation energies.

Lodders, K., & Fegley, B. (2025). Mineral condensation in stellar outflows. In *Presolar Grains in Extra-Terrestrial Materials: Probing Stars with Stardust* (pp. 539-583). Elsevier. https://doi.org/10.1016/B978-0-12-821830-3.00002-4. Revised 29 August 2024. Preprint.

Nucleation

Nucleation of presolar grains such as carbides, graphite and nitrides in stellar outflows involves formation of small crystals held together by strong valence forces and classical nucleation theory developed from terrestrial experiments on water must be modified to be applicable to CSE and SN ejecta (e.g., see Salpeter 1974, Cameron and Fegley 1982).The temperature depression (ΔT) below the equilibrium condensation temperature for condensation of nucleation seeds (aka condensation nuclei) is proportional to surface energy (γ_S) to the 1.5 power (Salpeter 1974, Cameron and Fegley 1982):

$$\Delta T \propto \gamma_S^{1.5}$$

Thus, larger surface energies give larger temperature depressions. The issues are that γ_S values are temperature – dependent, vary with crystallographic planes, vary with concentration of solutes (or impurities), and are poorly known. At absolute zero $\gamma_S = \gamma^\circ$, and at the critical temperature (T_C) $\gamma_S = 0$. Thus, to first approximation, the temperature dependence of the surface energy is (Bruce 1965)

$$\frac{d\gamma_s}{dT} \cong -\frac{\gamma^\circ}{T_C}$$

Some typical values for surface energies of presolar grain materials are tabulated below. Some sources give the temperature dependence, while others do not.

Table 1. Surface energies for some pure condensates in C- and O-rich CSE

Material	γ_s (erg cm^{-2})	Source
α–Al_2O_3 (0001 plane)	892 – 0.12T (°C)	Rhee 1972a
Os metal	1000	Palme and Wlotzka 1976
Graphite (c plane)	1059 – 0.113T (°C)	Rhee 1972b
Diamond (111 plane)	5400 @25 °C	Harkins 1942
TiC	1190±350 @1100 °C	Livey and Murray 1956
ZrC	800±250 @1100 °C	Livey and Murray 1956
β-SiC (110 plane)	3000 – 0.546T °C	Bruce 1965
TaC	1290±390 @1100 °C	Livey and Murray 1956
VC	1675±500 @1100 °C	Livey and Murray 1956

A literature search by Cameron and Fegley (1982) found the surface energies reported for corundum (α–Al_2O_3) vary from about 50 – 50,000 erg cm^{-2} (Duga 1969). As Cameron and Fegley (1982) noted, the extreme values are grossly in error, but plausible γ_S values of 300 – 600 erg cm^{-2}, still vary by a factor of two. Furthermore, γ_S values are decreased by impurities, e.g., aluminum, boron, carbon, nitrogen dissolved in SiC (Tanaka 2002, Pitthan et al. 2017), and various solutes (C, N, O, P, S, Si) dissolved in molten iron (Elliott et al. 1963). For example, at constant temperature in the 1450 – 1530 °C range, carbon concentrations of 0.1 – 0.5% lower the surface energy (tension) of molten iron at according to the equation:

$$\gamma_s = 1600 - 100(\%C)$$

Taken at face value one would expect disagreement between equilibrium condensation temperatures and the dust formation temperatures (locations) in CSE. Cameron and Fegley (1982) illustrate this for corundum condensation in the solar nebula (their Figure 6). But refer to Figure 8 of Lodders and Fegley (1997) that shows good agreement between the calculated and observed formation locations of dust in a CSE. Given the uncertainties in constraining surface energies of condensates, further discussion of nucleation constraints and of the more complicated nucleation models developed since Salpeter (1974) is beyond the scope of this review. We refer the reader to Bernatowicz et al. (1996, 2005) and Sedlmayr and Krüger (1997) who show good agreement between models and observations of presolar grains if certain conditions exist in CSE. However, see Chigai et al. (2002) for an alternative viewpoint.

With respect to formation times in SN ejecta, Cherchneff & Dwek (2010) note that "condensation from the gas phase is controlled by nonequilibrium chemically controlled nucleation processes, each of which has its own temperature dependence." This statement applies to non-static environments such as SN ejecta where physical conditions such as supersonic ejection flows, turbulent mixing, and radioactive heating superimpose additional controls on chemistry, and thus model uncertainties.

Photochemistry

Photochemical reactions in optically thin regions of a CSE and SN ejecta may drive disequilibrium chemistry if photochemical reactions times $t_{photo} < t_{chem}$, the thermochemical reaction times. The reaction time for an initial photochemical step, e.g.,

$$HCN + h\nu \rightarrow H + CN$$

$$t_{photo} = J^{-1}$$

is the inverse of the photodissociation rate constant J (s^{-1}),

$$J = \int_0^\infty \Phi_\lambda I_\lambda q_\lambda d\lambda$$

which is the convolution of wavelength (λ) dependent absorption cross sections (q), quantum yields (Φ), photon intensity (I) at a particular location in the CSE or expanding SN ejecta. The photon intensity (flux) is the ambient photon flux modified by scattering and absorption by gas and dust in the CSE or expanding SN ejecta. By analogy with planetary atmospheres (e.g., section 5.2 of Visscher et al. 2006), there should be a critical surface inside the CSE or ejecta at which thermochemical and photochemical time scales are equal, inward at higher temperatures and pressures where thermochemistry dominates and outward at lower temperatures and pressures where photochemistry dominates.

Condensates from Stars on the Red Giant Branch (RGB), Asymptotic Giant Branch (AGB), and Red Supergiants (RSG)

The O-rich and C-rich circumstellar envelopes of giant stars are rich in molecular gases (e.g., Ziurys 2006). Gases such as CO, HCN, SiO, SiS, CS, PO, PO_2, PS, PN, hydrocarbons, and molecules containing Al, Fe, and Na have been detected in O and C rich CSE (e.g., Olofsson 1997, Tenenbaum et al. 2010, Ziurys et al. 2018). Gas species change over wide ranges of total pressure and temperatures because monatomic, ionized, hydride, oxide, sulfide, halide, nitride *etc.* gases have different thermodynamic

stabilities, different reaction dependencies on total pressure, and their chemistry is coupled non-linearly.

The gas chemistry is important because it influences the condensation temperatures. For example, the metallic or metalloid elements e.g., Na, K, Rb, Cs, Ga, In, Tl, Ge, Sn, Pb, P, As, Sb, Bi, Au form molecular gases which is one reason why their condensation temperatures are lower than expected if they would condense as pure elements, as is the case for elements that mainly form monatomic gases. The more molecular gas species exist for an element, the more an element is retained in the gas phase. Therefore, is important to include as many gas species of an element as possible in the computations.

The condensate (host) minerals and condensation temperatures are fairly well known for solar-composition gas, however, the condensate phases and/or hosts for several trace elements at high C/O ratios remain unknown or uncertain and may involve exotic carbides, nitrides, sulfides, and alkali salts. Table 2 gives an overview of expected condensates in circumstellar shells and indicates which minerals have been observed in shells of red giant branch M and C stars and among some presolar grains.

Table 2. Major condensates in circumstellar envelopes (CSE) and presolar grains of giant stars[a]

		M-stars			C-stars		
E	Abund.[b]	Mineral; ideal formula	CSE	Grains	Mineral; ideal formula	CSE	Grains
O	1.41×10^{7}	oxides and silicates	…	…	Mg-Silicates	…	…
C	7.08×10^{6}	none expected	…	…	titanium carbide TiC[c]	√	√
					graphite C	√	√
					silicon carbide SiC[d]	√	√
					diamond?	√(?)	√
N	1.95×10^{6}	none expected	…	…	osbornite TiN[c]	…	…
					aluminum nitride AlN[c,f]	…	(√)
Mg	1.02×10^{6}	spinel $MgAl_2O_4$	√	√	niningerite MgS	√	…
		melilite **	√	√	spinel $MgAl_2O_4$	√	√
		forsterite Mg_2SiO_4	√	√	forsterite Mg_2SiO_4	√	√
		enstatite $MgSiO_3$	√	√	enstatite $MgSiO_3$[s]	√	√
		olivine $(Mg,Fe,Ni)_2SiO_4$[t]	√	√			
Si	1.00×10^{6}	melilite**	…	√	silicon carbide SiC[d]	√	√
		forsterite Mg_2SiO_4	√	√	iron silicide (Fe,Ni)Si	…	…
		enstatite $MgSiO_3$	√	√	forsterite Mg_2SiO_4[t]	√	√
		olivine $(Mg,Fe,Ni)_2SiO_4$[t]	√	√	enstatite $MgSiO_3$[s]	√	√
		SiO_2[r]	…	√			
Fe	8.38×10^{5}	iron alloy FeNi	…	√	iron metal[c]	…	√
		schreibersite $(Fe,Ni)_3P$	…	…	iron alloy FeNi	…	…
		olivine $(Mg,Fe,Ni)_2SiO_4$[t]	√	√	iron silicide (Fe,Ni)Si	…	√
		magnetite Fe_3O_4[e]	…	√ (?)	magnetite Fe_3O_4[e]	..	√ (?)
					olivine $(Mg,Fe,Ni)_2SiO_4$[t]	√	√
S	4.45×10^{5}	troilite FeS	√	√	oldhamite CaS[c,g]	…	(√)
					niningerite MgS	√	…
					troilite FeS	√	√
Al	8.41×10^{4}	corundum Al_2O_3	√	√	aluminum nitride AlN[c,f]	…	(√)
		hibonite $CaAl_{12}O_{19}$	√	√	corundum Al_2O_3	√	…
		grossite $CaAl_4O_7$	…	√	spinel $MgAl_2O_4$[u]	√	√
		melilite **	…	√	anorthite $CaAl_2Si_2O_8$	…	√
		spinel $MgAl_2O_4$	…	√			
		anorthite $CaAl_2Si_2O_8$	…	√			
Ca	6.29×10^{4}	hibonite $CaAl_{12}O_{19}$	√	√	oldhamite CaS[c,g]	…	(√)

		grossite $CaAl_4O_7$	…	√	anorthite $CaAl_2Si_2O_8$	…	…
		melilite	…	√			
		anorthite $CaAl_2Si_2O_8$	…	…			
Na	5.75×10^4	albite $NaAlSi_3O_8$	…	…	albite $NaAlSi_3O_8$	…	…
		halite NaCl	√	…	halite NaCl	√	…
Ni	4.78×10^4	kamacite & taenite	…	…	kamacite & taenite	…	√
		schreibersite $(Fe,Ni)_3P$	…	…	iron silicide (Fe,Ni)Si	…	…
		olivine $(Mg,Fe,Ni)_2SiO_4$[t]	√	√	schreibersite $(Fe,Ni)_3P$	…	…
Cr	1.29×10^4	Cr in FeNi alloy	…	…	daubréelite $FeCr_2S_4$	…	…
		Cr-spinel	…	√	$(Fe, Cr)_7C_3$[h]	…	√
					Eskolaite Cr_2O_3[e]	…	√ (?)
Mn	9.17×10^3	Mn_2SiO_4 in olivine	…	…	alabandite (Mn,Fe)S	…	…
P	8.37×10^3	schreibersite $(Fe,Ni)_3P$	…	…	schreibersite $(Fe,Ni)_3P$	…	…
		whitlockite $Ca_3P_2O_8$	…	…			
Cl	5.24×10^3	halite NaCl	√	…	halite NaCl,	√	…
		sylvite KCl	…	…	sylvite KCl	…	…
					djerfisherite $K_6Na(Fe,Cu,Ni)_{25}S_{26}Cl$	….	…
K	3.69×10^3	orthoclase $KAlSi_3O_8$	…	…	sylvite KCl	…	…
		sylvite KCl	…	…	djerfisherite $K_6Na(Fe,Cu,Ni)_{25}S_{26}Cl$	…	…
Ti	2.42×10^3	perovskite $CaTiO_3$	…	√	titanium carbide TiC	√ (?)	√
		other Ca-Ti-oxides	…		osbornite TiN[c]	…	(√)
		rutile TiO_2 [k]	…	√	rutile TiO_2[k]	…	√ (?)
		Ti oxides[w]	…	√			
Zr	10.9		…	…	ZrC[e,‡]	…	√ (?)
Mo	2.6		…	…	RMN[m]	…	√
Ru	1.81		…	…	Ru-Fe alloy[p]	…	√
Pt	1.24		…	…	RMN[m]	…	√
Os	0.652		…	…	Os-Mo-Ru-Fe[q] and RMN[m]	…	√
Ir	0.633		…	…	RMN[m]	…	√
W	0.144		…	…	RMN[m]	…	√

[a]Updated from Lodders and Amari 2005. Elements (column E) are in order of decreasing solar abundance. Condensates are in order of appearance with decreasing temperature for each element. A "?" means that entry is uncertain. (√) in parenthesis means that phase could be in solid solution or an exsolution product from solid solutions (e.g., AlN exsolved from SiC). [b]solar photospheric abundances where Si = 10^6 atoms. [c]See Lodders and Amari 2005 and Singerling et al. 2021. [d]See text and Hynes & Croat 2007, Hynes et al. 2007. [e]See Croat et al. 2008. [f]See Lodders & Amari 2005 and Stroud & Bernatowicz 2005. [g]See Lodders & Amari 2005 and Hynes et al. 2011. [h]Croat et al. 2005. [k]Croat 2007 [m]Croat et al. 2013a, RMN stands for refractory metal nuggets. [p]Croat et al. 2004 [q]Croat et al. 2005 [r]See Floss & Stadermann 2009, Nguyen et al. 2010, and Bose et al. 2012. [s]See Lodders & Amari 2005, Nguyen et al. 2013, Stroud et al. 2014, and Vollmer et al. 2007, 2013. [t]See Messenger et al. 2003, Stroud et al. (2014), Busemann et al. 2009, and Vollmer et al. 2009 who report olivines with variable Mg,Fe,Ni contents ranging from forsterite to more Fe and Ni rich. See Lodders & Amari 2005 and Nguyen et al. 2023. [w]Takigawa et al. 2014 report Ti oxides within a presolar corundum. [‡]Croat et al. (2008) state a single ZrC condensate "without any detectable Ti or Mo" was found but give no other details.
** Melilite is the solid solution of gehlenite $Ca_2Al_2SiO_7$ and akermanite $Ca_2MgSi_2O_7$.

Before proceeding we make a few comments about entries in Table 2. The Ru-Fe, Os-Mo-Ru-Fe alloys, and refractory metal nuggets (Os-Ru-Mo-Fe-Ir-W±Pt±Ni±Cr) reported by (Croat et al. 2004, 2005, 2013a) in graphite grains from AGB stars, supernova ejecta, and other source(s) are interesting because their compositions are qualitatively similar, but not identical to, those of refractory noble metal grains in Ca, Al-rich inclusions and predicted in solar nebula condensation sequences (e.g., Palme & Wlotzka 1976, Blander et al. 1980, Fegley & Palme 1985). With the exception of four nuggets analyzed by Croat et al. (2013), the major differences are the absence of Ir, Mo, Os, W from the Ru-Fe alloys and of Ir and W from the Os-Mo-Ru-Fe alloys. Iridium and Mo have volatilities similar to that of Ru and W has a volatility similar to that of Os so the absence of these metals may put important constraints on the temperature,

pressure, and composition conditions for formation of the observed grains. Croat et al. (2013a) present condensation calculations for refractory metals from a solar composition gas. However, these are not relevant to the case of RMN condensed in the circumstellar envelope of a carbon star or in supernova ejecta for two reasons. First, the RMN host phase graphite is not stable in solar composition gas. Second, the oxygen fugacity (fO_2) of the gas affects the gas and condensation chemistry of Mo, W, and other refractory metals (Fegley and Palme 1985, Fegley et al. 2023) and thus the computed composition of the RMN grains. The fO_2 of gas in the solar nebula is different than that of gas in the circumstellar envelope of carbon stars and of gas in the supernova ejecta because the H-C-O ratios are different. The Croat et al. (2013a) calculations are not a good match to the measured RMN compositions (even with only six of the nine metals in the grains being compared) or to our own results done at a C/O ratio of 1.2 with otherwise solar composition. New calculations with appropriate composition models for carbon star CSE and supernova ejecta are needed to explain the origin of the presolar refractory metal nuggets.

Table 2 lists several oxides found in presolar grains from carbon stars, e.g., silica SiO_2, magnetite Fe_3O_4, eskolaite Cr_2O_3, rutile TiO_2 (Croat 2007, Croat et al. 2008). The entries for the Fe, Cr, and Ti oxides are marked with a question mark because it is unclear if the oxides are actually indigenous to the presolar grain or contamination (see discussion in Croat 2007 and Croat et al. 2008). The oxygen isotopic composition of the magnetite, eskolaite, and rutile grains were not measured and cannot constrain the origin of the oxides. None of the four oxides are stable in condensation calculations at a C/O ratio of 1.2 in an otherwise solar composition gas, appropriate for modeling carbon stars (see later in this chapter). Titanium remains in TiC, Cr condense into metal alloy, Fe condenses as FeSi and metal alloy, and Si condenses as SiC, FeSi, and as magnesian silicates at low temperatures. Silica is unstable in a gas with a Mg/Si ratio >1 because magnesian silicates such as $MgSiO_3$ can form. Pure silica could be stable in a gas with excess Si because all Mg could be bound in $MgSiO_3$ for example leaving excess Si for SiO_2 formation.

Physical Setting in Circumstellar Envelopes

Grain formation in CSE is observationally confirmed and facilitates mass loss from the star into the interstellar medium. Mass loss is driven by stellar radiation pressure onto the grains which drag the surrounding gas along by momentum coupling. Many AGB stars are pulsating variable stars with variability periods around one year. (These variations are not to be confused with the thermal pulses from alternating H and He shell burning in the stellar interior on ~10,000-year timescales.) Maximum luminosity is reached near maximum surface temperature and minimum radius. Between maximum and minimum, temperatures characteristically vary by $\leq$ 10% (200-400K) but the radius may vary by >20% ($\Delta \approx$ 0.5 AU). Thus, any dust has to form within a year or less for dust-driven wind to work and to prevent fall-back of matter and dust evaporation from the CSE during minimum radius and highest temperatures in the pulsation cycle.

Temperatures and total pressures in circumstellar shells are estimated from about 2000-2500K and 10^{-5} bar near the photosphere and rapidly decrease to around <300K and < 10^{-10} bar with radial distance from the star. Some model P-T structures and more references to them are described in e.g., Bernatowicz et al. 1996, Sharp & Wasserburg 1995, Lodders & Fegley 1995, 1997, 1999; Lodders 2008. For illustrative purposes, results below are given for 10^{-5} bar total pressure. The condensation sequence is not strongly affected by lower total pressure; however, the condensation temperatures usually drop when the total pressure is decreased.

Condensation for a Solar Gas

The condensation chemistry from a solar composition gas has been discussed extensively (Larimer (1967, 1973), Larimer & Anders (1967), Grossman (1972), Grossman & Larimer (1974), Boynton (1975), Wai & Wasson (1977, 1979), Sears (1978), Fegley & Lewis (1980), Saxena & Eriksson (1983a,b), Fegley & Palme (1985), Kornacki & Fegley (1986), Palme & Fegley (1990), Wood & Hashimoto 1993, Yoneda & Grosman 1995, Ebel 2000, Ebel & Grossman 2000, Lodders 2003, Fegley & Schaefer 2010, and comprehensive reviews by Ebel 2006, 2021). These computations serve as a baseline for the expected condensates in other solar composition-like systems. As long as compositions are H and He rich and relative elemental abundances of major elements are near-solar and C/O ratios <1, the type of condensates are essentially the same as those computed for a standard solar gas. Figure 2 shows the major condensates and their stability regions for solar elemental composition as a function of temperature and total pressure (see Ebel 2006 for similar Figures and discussion).

Major element condensation temperatures strongly increase with log total pressure. Aluminum – bearing compounds are the highest temperature condensates. Corundum is first at the lowest total pressures and is replaced by hibonite and grossite with increasing total pressure. On the other hand, with decreasing temperature at a given total pressure, the Al-bearing condensate is replaced by successively more complex compounds, e.g., corundum transforms into hibonite, then hibonite + grossite, then grossite + melilite (a solid solution of gehlenite and akermanite), then melilite + hibonite, then melilite + corundum (low P) or melilite + spinel (higher P) before anorthite replaces melilite. There are also condensation curves to show the temperatures below which Fe-metal, forsterite and enstatite are stable.

At total pressure conditions relevant to stellar outflows (about < 10^{-4} bar) the condensation sequence becomes less complex, e.g., only small stability range "wedges" exist for grossite (not present below 10^{-7} bar) and spinel (not present below 10^{-5} bar). At the lowest total pressure shown, corundum, hibonite, melilite, and anorthite are the Al-bearing condensates. Corundum and hibonite are known among presolar grains from RSG and AGB stars consistent with the estimated low total pressure regime in the circumstellar environment, and rare occurrence of grossite among presolar grains (one case known, see Vollmer et al. 2009) from such sources would also be consistent. In contrast, the observed spinel grains (if from RGB and AGB sources) would suggest that higher total pressures are reached in the circumstellar shells, but it would then leave the mystery why grossite grains are so elusive.

However, metallicity (element/H abundance ratio for elements heavier than He) is also important in determining the condensation sequence. Results for the same computation as shown in Figure 2b but for 10x solar metallicity show that spinel stability increases to around 10^{-7} bar within the condensation sequence (Figure 2c). Almost all stability regions for solar conditions shift to lower total pressure and higher temperatures when the metallicity is increased. Conversely, a decrease in metallicity shifts the boundaries toward higher total pressures and lower temperatures (Figure 2a).

Metallicity also affects the condensation temperatures of other phases such as forsterite, enstatite, anorthite, diopside and Fe metal. Table 3 provides fits to starting condensation temperatures of several major condensates; these fits reproduce the condensation temperatures within about 5K.

The fits are in the form:

$10^4/Tcond = A + B \log P_{tot} + C [M/H]$

where Tcond is the starting condensation temperature in K, log P_{tot} is the decadic logarithm of the total pressure in bar, and [M/H] is the decadic logarithm of the factor for the change in all elemental abundances from solar for all elements heavier than helium (e.g., [M/H] = -1 for a ten-times decrease in metallicity from solar).

These fits should not be extrapolated beyond their indicated validity range because other phases may become stable, as shown in Figure 2, e.g., the corundum stability field is limited by the appearance of hibonite as the initial Al-bearing condensate. Also note that corundum appears twice in the condensation stability sequence at a given total pressure. First as the initial condensate, and second when hibonite reacts away to melilite to leave corundum at lower temperatures. The fits are only for the first appearance temperature of a given phase.

Figure 3 shows which initial Al and Ti bearing condensates are present as a function of total pressure and metallicity. Figure 3a shows that corundum is the first Al-bearing condensate at low total pressures for a wide range in metallicity and is also favored towards higher total pressures at the lowest metallicity shown. Hibonite behaves similarly at total pressures around the 1 bar level. At the highest total pressures shown, grossite, melilite and $CaAl_2O_4$ (krotite) appear as the first Al-bearing condensates, and the initial condensates have higher Ca:Al ratios than hibonite. The dotted lines are isotherms for the starting (aka appearance) condensation temperatures in 100K steps as indicated. The distances between the almost parallel running isotherms narrow with increasing temperature which reflects the inverse condensation temperature dependence on log P_{tot} and metallicity (equation above).;

Table 3. Condensation temperatures of major phases as a function of total pressure and metallicity: $10^4/T_{cond}(K) = A + B \log P_{tot} + C [M/H]$ for total pressures < 10^{-3} bar and solar C/O

Phase	A	B	C	Comments
Al_2O_3	5.014396	-0.238925	-0.616745	corundum initial Al condensate
$CaAl_{12}O_{19}$	4.825490	-0.337694	-0.674237	hibonite stable as 1st or 2nd Al-bearing condensate
Melilite	5.292832	-0.318888	-0.637370	
Spinel	5.667352	-0.374511	-0.742036	
Mg_2SiO_4	5.901353	-0.369365	-0.728550	
$MgSiO_3$	6.229913	-0.349652	-0.685978	
$CaAl_2Si_2O_8$	5.981157	-0.321792	-0.655161	anorthite stable before diopside
$CaMgSi_2O_6$	5.995771	-0.342130	-0.690781	diopside stable after anorthite
Fe-alloy	5.401515	-0.492346	-0.5003467	Pure iron as proxy here*
FeS	14.19900	0	-2.829900	
$CaTiO_3$	5.112903	-0.291241	-0.530776	perovskite as initial
Ti_2O_3	5.173840	-0.290171	-0.434175	tistarite as initial
TiN	5.265570	-0.428886	-0.217314	osbornite as initial

Maximum uncertainty ± 10 K. * Fe metal also starts to condense into refractory alloy at higher temperatures.

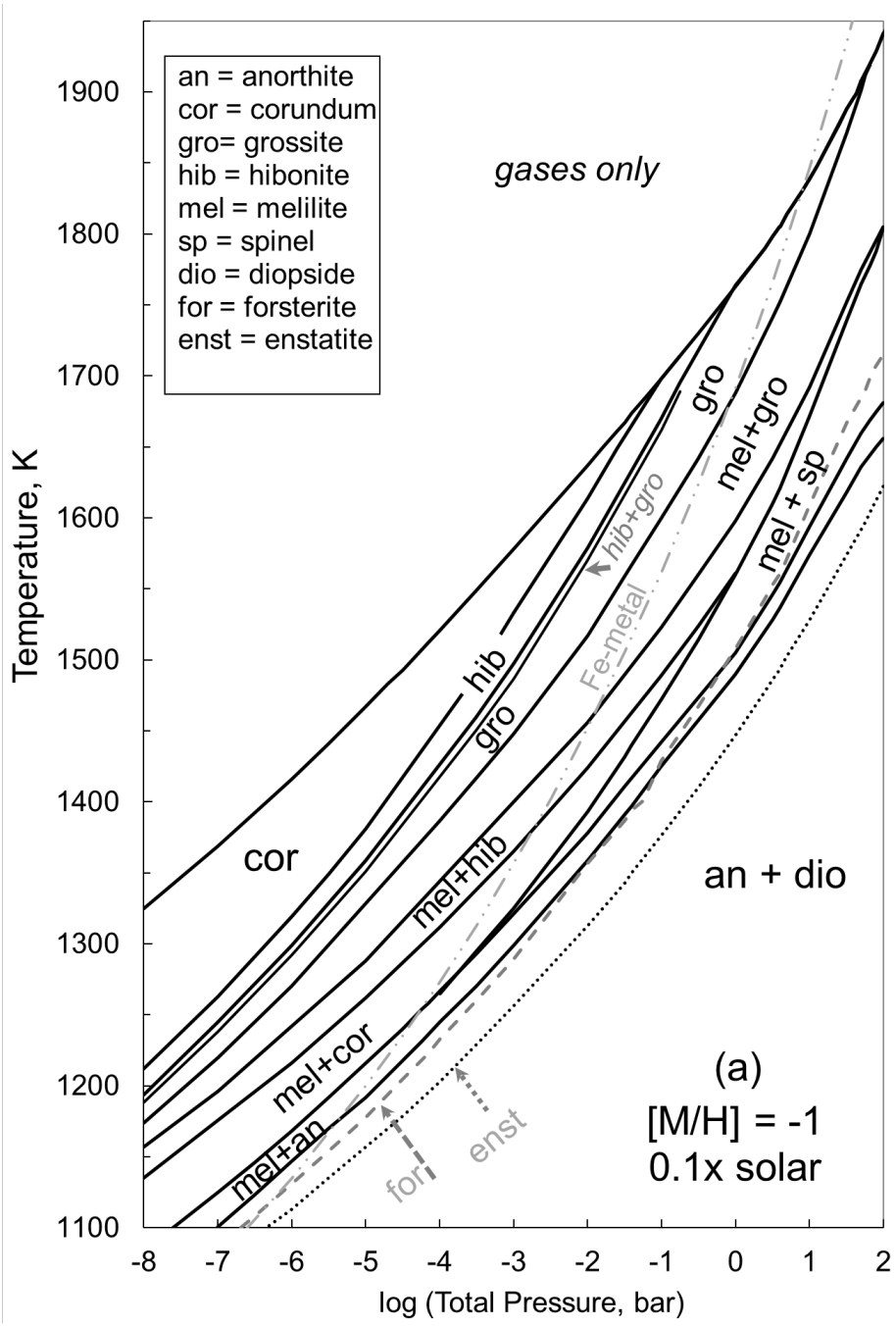
an = anorthite
cor = corundum
gro= grossite
hib = hibonite
mel = melilite
sp = spinel
dio = diopside
for = forsterite
enst = enstatite
gases only
cor
hib
gro
mel+hib
mel+cor
mel+an
hib+gro
gro
mel+gro
mel + sp
Fe-metal
for
enst
an + dio
(a)
[M/H] = -1
0.1x solar
Temperature, K
log (Total Pressure, bar)
1900
1800
1700
1600
1500
1400
1300
1200
1100
-8
-7
-6
-5
-4
-3
-2
-1
0
1
2

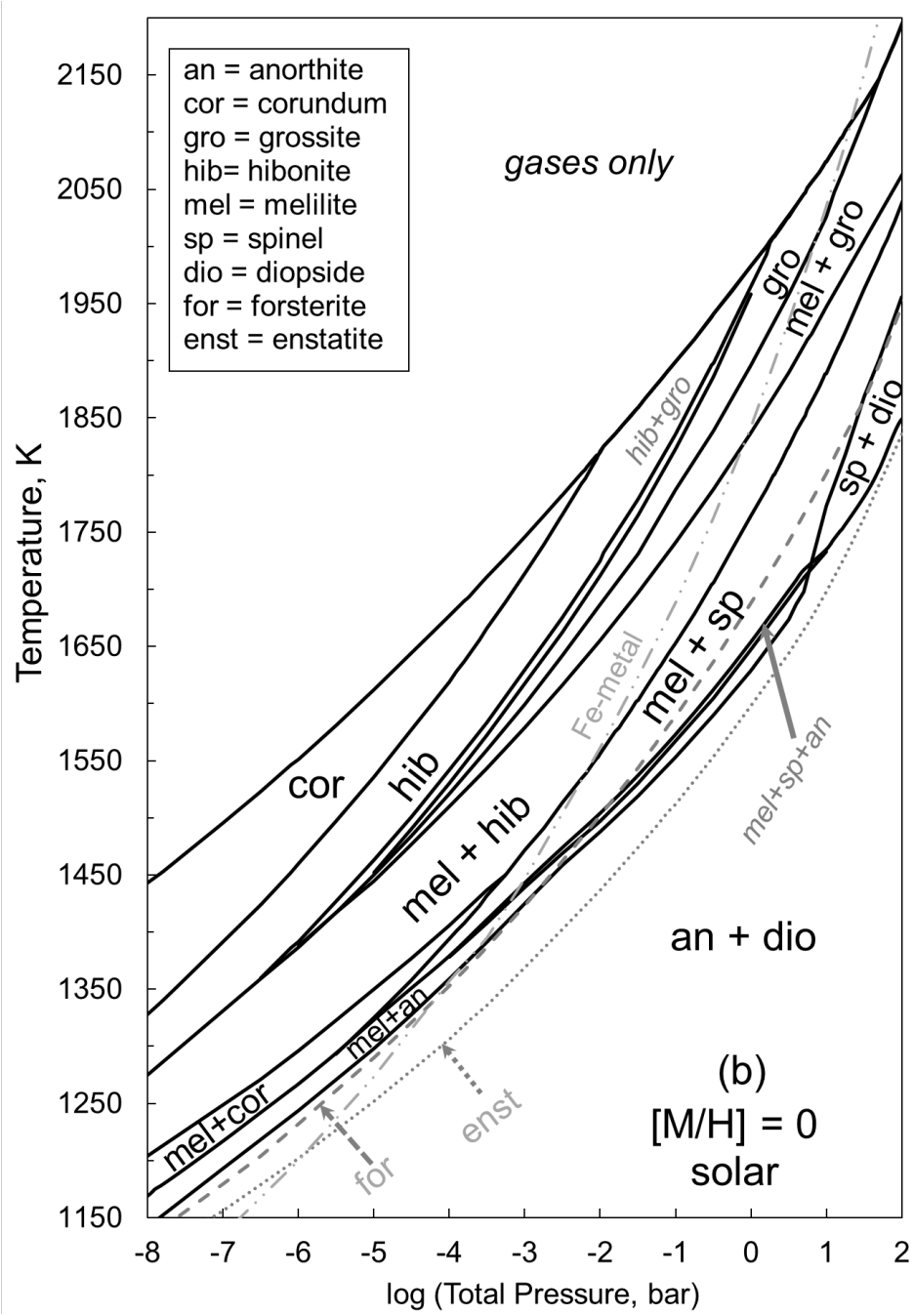
an = anorthite
cor = corundum
gro = grossite
hib= hibonite
mel = melilite
sp = spinel
dio = diopside
for = forsterite
enst = enstatite
gases only
cor
hib
mel + hib
mel+cor
mel+an
hib+gro
gro
mel + gro
Fe-metal
mel + sp
sp + dio
mel+sp+an
for
enst
an + dio
(b)
[M/H] = 0
solar
Temperature, K
log (Total Pressure, bar)
2150
2050
1950
1850
1750
1650
1550
1450
1350
1250
1150
-8
-7
-6
-5
-4
-3
-2
-1
0
1
2

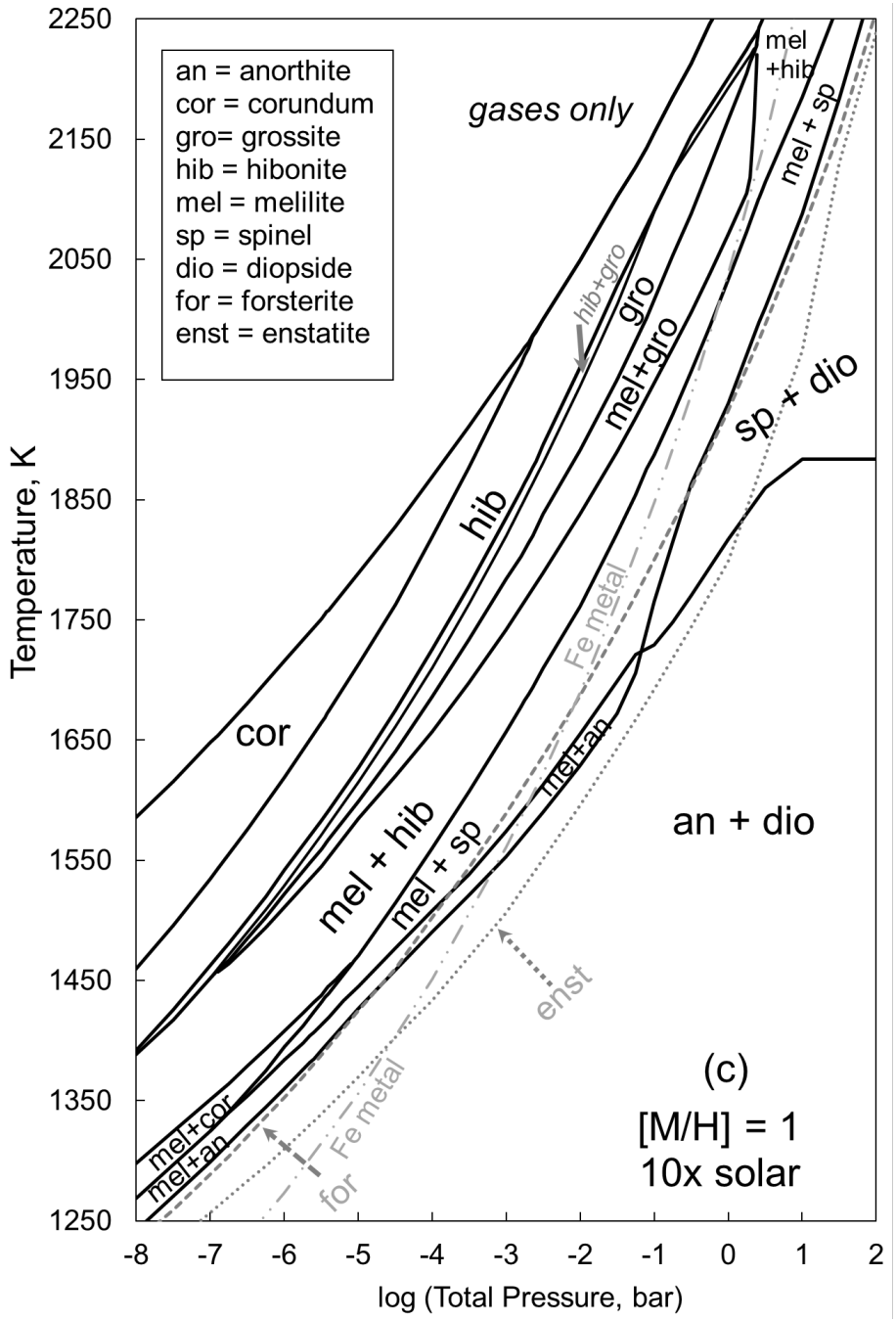

Figure 2a-c: Calcium and aluminum condensates and their stability regions as a function of temperature and total pressure at metallicities 0.1, 1, and 10 times the solar metallicity. Condensation temperatures of enstatite, forsterite, diopside and Fe-metal are also shown. Note the decreasing temperature ranges on the ordinates. The stability range of Ca-aluminates increase with increasing metallicity into lower total pressure ranges. Grossite (Gro) is stable in different phase assemblages and listed several times.

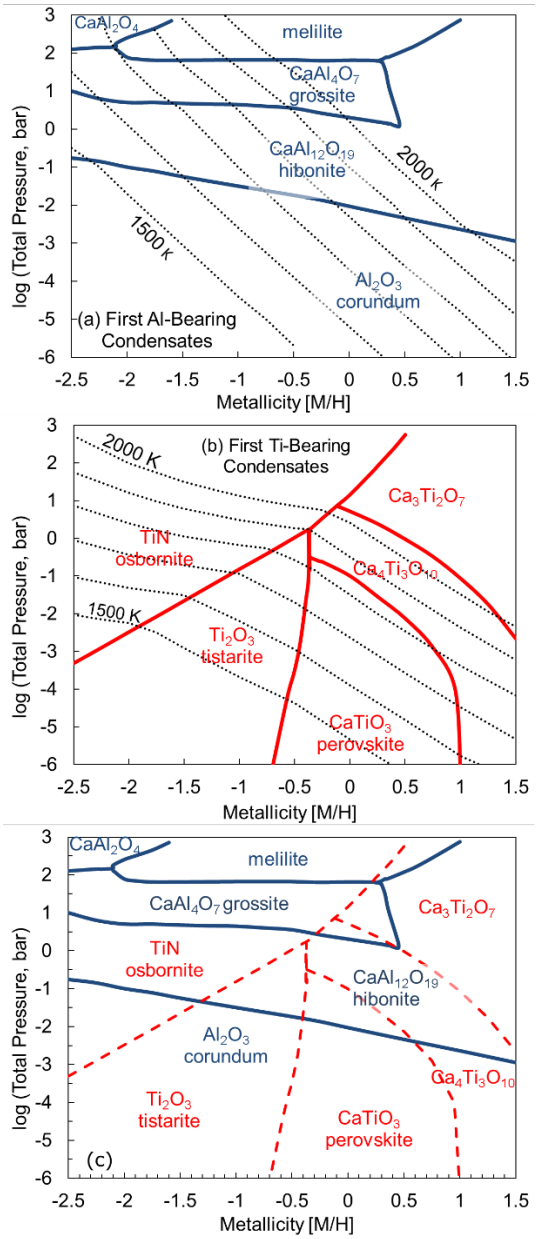

Figure 3 a-c. Stability fields of initial Al- and Ti- bearing condensates as a function of total pressure and metallicity. Plots (a) and (b) show isotherms (dotted curves) for the starting condensation temperatures in 100K steps. Graph (c) shows the combined fields for Al and Ti, which illustrate the interdependence of the stability of Ca-Al- and Ca-Ti-oxides as they compete for Ca. See text for more details.

Figure 3b shows which Ti-bearing condensate appears first as a function of total pressure and metallicity. The diagonal divides the log P and metallicity space where the titanium nitride osbornite is the first condensate (towards lower metallicity and higher total pressures) versus Ti_2O_3 (tistartite) and

Ca-Ti-oxides. In TiN and Ti_2O_3 titanium is trivalent, which is favored at lower metallicities because there is a decrease in the H_2O/H_2 ratio with metallicity. Titanium is tetravalent in perovskite, and Ti^{3+} and Ti^{4+} are both present in $Ca_3Ti_2O_7$ and $Ca_4Ti_3O_{10}$. The latter two Ca-Ti oxides are the initial condensates at higher total pressures and metallicities and probably not to be expected as presolar grains as frequently as one would expect perovskite and Ti_2O_3, which have larger stability ranges towards lower total pressures. The dotted curves are isotherms for the starting condensation temperatures of the different initial Ti-bearing condensates. The narrowing between the parallel isotherms with increasing temperature is the same as described for Al above. In contrast to Al, for Ti the slopes of the curves become steeper when they cross over the diagonal divide from TiN to oxide condensates.

Aluminum and titanium chemistry are linked through the competition for Ca between the Ca-Al and Ca-TI bearing condensates. This is the reason for the wedge shape of the field for grossite in Figure 3a as initial condensate. The very first Al-bearing and Ti-bearing condensates as a function of total pressure and metallicity are shown in Figure 3c.

The highest temperature condensates are ultrarefractory trace element oxides and noble metal alloys. Their condensation temperatures as a function of total pressure and metallicity are of particular interest because these may serve as nucleation seeds for other condensates at lower temperatures. This has been inferred for reduced condensates (C/O > 1) where refractory Ti-Zr-Mo-carbides are observed at the centers of graphite grains (Bernatowicz et al. 1996, Croat et al. 2003a and below).

Analogous grain within grain configurations for oxidized condensates with C/O <1 could consist of ultrarefractory trace and major element condensates similar to those known from ultra-refractory Ca-Al-rich inclusions (CAIs) seen in chondritic meteorites. However, one might expect ZrO_2(-rich) presolar grains or Os-rich metal grains as internal sub-grains in presolar Ca-Al-Ti oxide grains. Such grains have not yet been reported among presolar oxides. The absence (if real) of such oxide nucleation seeds could be due to formation of solid solutions and/or resorption of ultrarefractory trace element oxides into slightly less refractory major element oxides such as corundum, hibonite or perovskite. There are no oxide nucleation seeds but there are refractory metal grains in the RNZ inclusion from Ornans, which has large enrichments of 10,000 times solar for Lu and Hf and 15,000 times solar for Re and Os (Palme et al. 1982). We note the metal inside oxide scenario for oxidized CSE grains is qualitatively similar to coexistence of two separate carbide and graphite phases in reduced presolar grains.

The Effect of C/O Ratio on Condensates

When stars return most of their mass back to the interstellar medium, the elemental composition of these ejecta determines which types of condensates can form. The ratio of the total carbon and oxygen abundances (C/O ratio) is important because their chemistry determines the oxidation state of the gas. The formation of oxides and silicates involve reactions with water vapor, and it is therefore practical to use the H_2O/H_2 ratio as a proxy for the oxidation state. For example, corundum formation from AlO (g) can be written as

$$2\ AlO\ (g) + H_2O\ (g) = Al_2O_3\ (corundum) + H_2\ (g)$$

leading to an equilibrium constant (K_{eq}) expression for the thermodynamic activity of corundum:

$$a_{Al_2O_3} = K_{eq} \frac{P_{AlO}^2 P_{H_2O}}{P_{H_2}}$$

The activity of pure corundum is unity at (and below) its condensation temperature and less than unity above that point. The H_2O/H_2 ratio depends on how much oxygen is available to form H_2O (g), which depends on the oxygen abundance and on how much oxygen is in the very stable carbon monoxide (CO) gas. At the same time, the amount of CO (g) also depends on the carbon abundance. The following reactions illustrate the competition of CO and H_2O for oxygen:

$$CO\ (g) + 3\ H_2\ (g) = H_2O\ (g) + CH_4\ (g)$$

and

$$2\ CO\ (g) + 3H_2\ (g) = 2\ H_2O\ (g) + C_2H_2\ (g)$$

In solar-like systems with C/O < 1, the major O-bearing gases are thus H_2O(g) and CO, which is essentially inert because of the high C≡O bond energy. Other O-bearing gases such as SiO(g) are typically less abundant oxide gases. Conversely at C/O > 1, CO is the only major O-bearing gas.

As a rough guideline, both equilibria are shifted to the left above 1000 K and total pressures below one mbar; at lower temperatures and higher total pressures the equilibria shift to the right but in practice this shift becomes more kinetically controlled as temperatures drop (see Lodders & Fegley 2002 for a detailed discussion of the T, P and abundance dependent C, N, and O chemistry).

Figure 4 shows the starting condensation temperatures for corundum and other major condensates as a function of the bulk C/O ratio at constant total pressure of 10^{-5} bar. The condensation temperatures were calculated by increasing the carbon abundance in an otherwise solar gas. In RSG and AGB stars, nitrogen is also enhanced over solar, but the N abundance was not changed for the calculations in Figure 4; some effects of increased N abundance are described below.

The types of condensates from a gas with variations in C, N, and O abundances from solar composition gas remain similar to those computed for a gas of solar composition as long as C/O < 1. The major condensates involve rocky elements high in relative abundance such as Si, Mg, Al, Ca, Na and Ti which serve as cations, and O serves as anion (O^{2-}) in oxides; more complicated anion structures such as $(SiO_4)^{4-}$ and $(AlO_4)^{5-}$ are involved in silicates but also obtain their negative charges from oxygen; the third most abundant element after H and He in solar-like compositions.

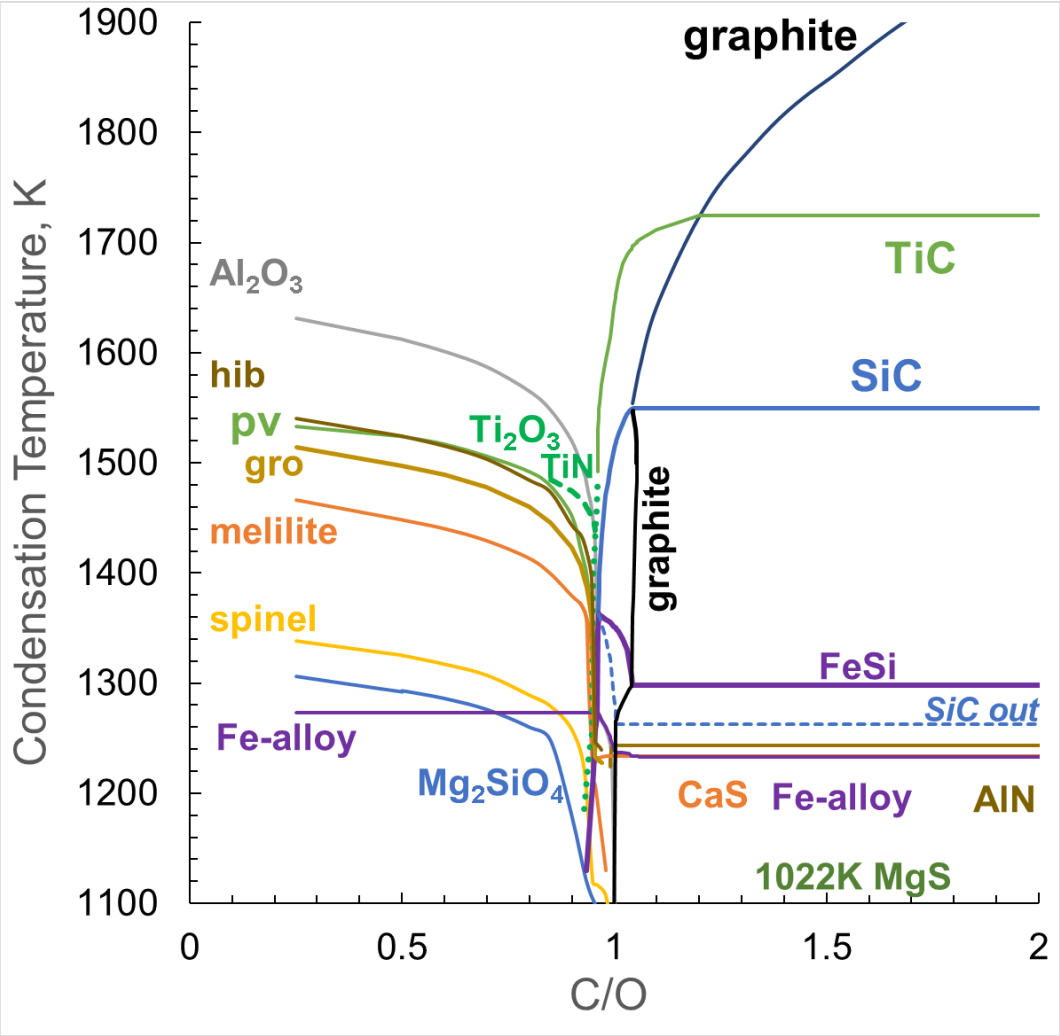

Figure 4. Selected condensation temperatures of major elements as a function of C/O ratio at 10^{-5} bar total pressure. The C/O was increased by increasing the C-abundance. Oxide and silicate condensation temperatures drop as the solar C/O around 0.5 is increased. The steep drop near C/O = 1 is caused by the paucity of H_2O as essentially all O and C are bound in the very stable CO molecule. At C/O > 1 the condensation temperatures for C-bearing compounds increase with C/O as more free carbon (not tied to CO gas) becomes available. Note the constant Fe alloy and FeSi condensation temperatures at C/O<1 and C/O>1, respectively. The CaS (oldhamite), Fe-alloy, and AlN (aluminum nitride) condensation temperatures above C/O >1 are independent of C/O and coincide within a few degrees at this total pressure. Niningerite, MgS, condenses at 1022K independently of C/O as long as C/O>1. The dotted line "SiC out" indicates where SiC disappears.

Most noticeable in Figure 4 is the drop in condensation temperatures of oxides and silicates as the C/O ratio increases. This can be explained as follows. At high temperatures of interest for C/O < 1, all carbon is tied into CO, and the amount of oxygen in water is about the difference between oxygen and carbon abundances ($eH_2O = eO – eC = eO - eCO$, where eX stands for the abundance by number). The solar C/O

is about 0.5; thus, half of the oxygen is in CO (g) and the other half in H_2O (g) (the amount of O in other gases such as SiO is small by comparison). With increasing C/O ratio, the amount of O in H_2O decreases, which means that the H_2O/H_2 ratio drops in reactions such as shown above for corundum (at otherwise constant P and T). This means that the activity (the proxy for stability) of corundum drops and therefore the condensation temperature of corundum decreases with increasing C/O ratio.

The major effects seen from Figure 4 are a general decrease in condensation temperatures from solar with C/O ratios increasing towards unity, and an increase in or constant condensation temperatures after the minimum as C/O ratios raise above unity. In addition, there is a gradual change in initial condensates from oxidized to reduced mineralogy. Titanium condensation behavior is illustrative for this as Ti has oxidation states 3+ and 4+. At solar C/O, the initial condensate is perovskite, $CaTi^{4+}O_3$. The condensation temperature drops because the H_2O(g) abundance decreases as more O is tied to CO(g) with increasing carbon abundance, resulting in a net decrease in H_2O/H_2 gas abundances. Therefore, the equilibrium

$$Ca\ (g) + TiO\ (g) + 2\ H_2O\ (g) = CaTiO_3\ (perovskite) + H_2\ (g)$$

shifts to the left at a given temperature and lower temperatures are needed to stabilize (i.e., reach the same thermodynamic activity of) perovskite. Around C/O of 0.9, the more reduced Ti_2O_3 is the first condensate with oxidation state Ti^{3+}. Another way to look at this is that the number of H_2O required per one Ti condensed is lower with Ti^{3+} than with Ti^{4+},

$$TiO\ (g) + 0.5\ H_2O\ (g) = 0.5\ Ti_2O_3\ (tistartite) + 0.5\ H_2\ (g).$$

This reaction also shifts to the left with increasing C/O (decreasing H_2O/H_2 gas abundances). The higher C/O also decreases the TiO(g) abundance at the expense of monatomic Ti(g) producing H_2O, however, the resulting condensation reaction

$$Ti\ (g) + 1.5\ H_2O\ (g) = 0.5\ Ti_2O_3\ (tistartite) + 1.5\ H_2\ (g)$$

then requires more H_2O for Ti_2O_3 formation, leading to the same result as writing the condensation reaction with TiO(g). This is a consequence of the path-independence of coupled reactions at chemical equilibrium.

Around C/O = 0.95 to 0.96, the H_2O/H_2 ratio is too low for the condensation reaction of Ti_2O_3 to compete with TiN condensation. The minimum condensation temperature in Figure 4 is where both trivalent Ti -bearing condensates coexist:

$$0.5\ Ti_2O_3\ (tistartite) + 0.5\ N_2\ (g) + 1.5\ H_2\ (g) = TiN\ (osbornite) + 1.5\ H_2O\ (g)$$

The condensation reaction

$$TiO\ (g) + 0.5\ N_2\ (g) + H_2\ (g) = TiN\ (osbornite) + H_2O\ (g)$$

produces H_2O and does not consume it as in the condensation reactions for lower C/O. With further increase in C/O, the TiN condensation temperatures increase because there is less H_2O(g) and the condensation reaction shifts to the right. However, there is only a very small range in C/O where TiN is the first Ti-condensate and before TiC takes over.

On the other hand, if C/O >1, all oxygen is in CO(g) and carbon is mainly present in the gases acetylene (C_2H_2), C_2, CN, HCN, but also SiC_2 and many other minor organic compounds. This reducing gas composition favors condensation of elemental carbon as graphite or amorphous carbon, and covalently bound carbides such as SiC, TiC, and ZrC.

Among the major C-bearing condensates (TiC, C or SiC) the first ones show a strong increase in condensation temperature with C/O ratio (see also the detailed discussion in Lodders and Fegley 1995). As shown in Figure 4 near C/O = 0.95 to <1, TiC and SiC condense at higher temperatures than graphite, but with C/O > 1 graphite condensation temperatures steeply increase and surpass those of TiC and SiC. Once graphite is stable, the condensation temperatures of TiC and SiC become constant independent of C/O ratio. The reason for this is that the carbon activity is fixed at unity so that the condensation reaction is

$$\text{C (graphite)} + \text{Ti (g)} = \text{TiC (s)}$$

For which the equilibrium constant expression, solved for the activity of TiC is:

$$a_{TiC} = K_{TiC}\frac{X_{Ti}P_{Tot}}{a_{graphite}} = K_{TiC}X_{Ti}P_{Tot} = K_{TiC}C'$$

only dependent on the Ti (g) partial pressure, which can be written as product of the Ti gas mole fraction X_{Ti} and total pressure. Chemical equilibrium calculations show there are no other major Ti-bearing gases that could be affected by the C/O ratio and the total pressure is kept constant in Figure 4, so P_{Ti} is a constant denoted C′. The equilibrium constant is likewise constant at a given temperature; hence the TiC activity is constant at a given temperature and is invariant with C/O ratio. As temperature decreases the TiC activity increases until the critical isotherm where unit activity occurs and TiC condenses.

For SiC, a similar analysis yields the same conclusion. However, there are several different Si-gases that are more (or less) abundant, which are Si (major reservoir), some SiS, and minor amounts of SiC_2 gas. Lodders and Fegley (1995) describe the Si gas chemistry in detail and showed that only about 56% of all Si can condense into SiC because SiS remains in the gas until there is a condensate that will also remove sulfur. An increase in C/O does not affect the SiC_2 gas abundance significantly. There is a simple reason for this invariance. The net thermochemical reaction forming SiC_2 gas can be written as

$$2\ \text{C (graphite)} + \text{Si (g)} = \text{SiC}_2\ \text{(g)}$$

The partial pressure of SiC_2 gas is given by the equation,

$$P_{SiC_2} = K_{eq}P_{Si}a_{graphite}^2$$

The thermodynamic activity of graphite – not its abundance – is the key variable controlling the SiC_2 partial pressure. The activity of graphite is constant at unity in the graphite stability field; $a_{graphite}$ does not depend on the C/O ratio as long as graphite is present. In turn, once graphite and SiC are both condensed, the Si gas pressure is invariant and is controlled by the equilibrium:

$$\text{SiC (s)} = \text{C (graphite)} + \text{Si (g)}$$

so the Si(gas) abundance will not be lowered by removal of Si into SiC_2 gas.

Lodders, K., & Fegley, B. (2025). Mineral condensation in stellar outflows. In *Presolar Grains in Extra-Terrestrial Materials: Probing Stars with Stardust* (pp. 539-583). Elsevier. https://doi.org/10.1016/B978-0-12-821830-3.00002-4. Revised 29 August 2024. Preprint.

Metallicity Effects on C, TiC, and SiC Condensation

The condensation temperature sequence of TiC, C, and SiC can be inferred from the structure of many presolar grains from C-rich AGB stars (Lodders & Fegley 1995, 1997, Bernatowicz et al. 1996). From high to low temperatures the sequence is TiC (or some (Ti,Zr,Mo) carbide), graphite, and SiC. The first formed condensate is usually some refractory transition metal carbide composed of (Ti,Zr,Mo)C found near or close to the center of graphite grains, which suggests that these carbides acted as nucleation seeds for graphite. The refractory transition metal carbides may also serve as nucleation seeds for SiC but they form a solid solution, so refractory metal carbides (not dissolved or newly exsolved upon cooling) within SiC could be scarce.

Silicon carbide is usually absent from such graphite grains. The occurrence of SiC within graphite is rather rare (only 1-2 instances have been observed) suggesting that commonly, graphite condenses prior to SiC. This is in stark contrast to the incorrect notion that carbon can only condense at lower temperatures (1100 K) than SiC (1400K) (Ferrarotti and Gail (2001, 2006) and is unfortunately still assumed in dust modelling (e.g., see chapter by Lugaro et al., this volume.)

This sequence (TiC – graphite – SiC) constrains the total pressure conditions under which these grains condensed in the circumstellar shells to about 10^{-4} to 10^{-5} bars, as concluded previously, assuming that the grains originated from solar-metallicity stars. However, as shown in Figure 5, the observed sequence also depends on the metallicity of the stellar sources. Reducing the solar metallicity by a factor of ten shows that the sequence TiC, C, and SiC only occurs in a total pressure interval of about 10^{-5} to 10^{-7} bars, and if the solar metallicity is reduced by a factor of 100, pressures less that about 10^{-6} to 10^{-9} bars are needed.

At lower metallicities and higher total pressure, the sequence of TiC, SiC, and C is expected. Titanium carbide can dissolve in SiC and the observed Ti/Si ratios in many SiC grains are consistent with this condensation sequence. However, the caveat is that SiC grains are very rarely observed within graphite grains, which indicates that the condensation sequence TiC - SiC - C was not the main condensation path for the majority of known presolar dust. One possible answer is that kinetic inhibition at low temperatures prevented carbon from condensing onto pre-existing SiC grains. However, this can be ruled out because more volatile trace elements are condensed into SiC. If more volatile, less abundant elements made it into the SiC, the more abundant, more refractory carbon is expected as well.

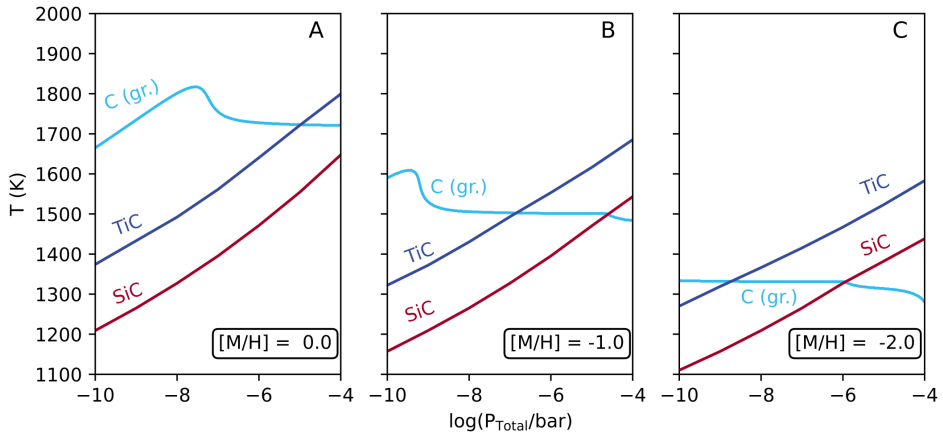

Figure 5. The condensation temperatures of TiC, C, and SiC as a function of total pressure for solar ([M/H] = 0, 0.1x [M/H] = 0.1), and 0.01x solar ([M/H] = -2) metallicity at a C/O ratio of 1.2 (Adams and Lodders 2024).

Effects of Increased N Abundances on Condensate Stability

The influence of the N abundance on condensate stability is described in detail in Lodders & Fegley (1995) and only briefly noted here. An increase in N abundance over solar values increases the relative abundances of all N-bearing gases according to the Le Chatelier principle, e.g., the net thermochemical reaction for the production of HCN observed in AGB stars:

$$CO + 0.5\ N_2 + 1.5\ H_2 = HCN + H_2O$$

in M, S, and C stars; and for C stars also the net thermochemical reaction

$$C_2H_2 + N_2 = 2\ HCN.$$

These gas phase reactions shift to the right with higher N abundances (most N is in N_2 at temperatures and pressures where mineral condensation takes place) and explain the relatively high HCN gas abundances observed in AGB stars, in particular those with higher C/O ratios.

At C/O < 0.95, enhancements in the nitrogen abundance in red giants generally do not affect the condensate species because there are no nitride gases that are more stable than the oxide gases or oxidic condensates, which many elements form in a cooling gas of solar composition. The major effect of enhanced nitrogen abundances is a modest increase in total pressure as the addition of an essentially "inert" gas (N_2) only increases the number density, hence total pressure.

At C/O > 0.95, a higher N abundance increases the stability and thus condensation temperatures of N-bearing condensates such as TiN, AlN, and Si_3N_4. Nitrides are usually not among the first condensates for solar-like C/O ratios (see Figure 2) but begin to appear as first condensates (TiN, AlN) in the condensation sequence when C/O ratios approach unity (Figure 4). However, at C/O above unity, TiN is replaced by the more stable TiC and only AlN remains as the first condensate for Al. The AlN condensation temperature increases with increasing N abundance. For example, at C/O = 1.05 and 10^{-5} bar, the AlN condensation temperature increases from the solar value of 1242K to 1266K (10x solar N) and to 1291K (100x solar N). Like other nitrides with NaCl structure, AlN may condense into solid solution with SiC (which is stable at higher temperatures) and an increased N abundance facilitates higher N-contents in SiC grains. This is of interest because of N-isotopic measurements in SiC grains.

Another effect of increased N abundance is a decrease in graphite and SiC stability because of the formation of HCN. This is very pronounced for graphite at higher total pressures where graphite is no longer stable at 0.01 bar for N-enhancements above 10x solar. Around 10^{-5} bar the graphite condensation temperature drops from 1600K to 1553K (10x solar N) and 1390K (100x solar N at C/O = 1.05). Only at very low total pressures (10^{-12} bar), the graphite condensation temperature drop (due to a higher N abundance) become negligible because the total pressure dependence in the HCN formation reaction is less effective. For SiC, the decrease from the condensation temperature of 1544K (solar N) is about 20K per factor of ten N-enrichment over solar at C/O = 1.05 (Lodders & Fegley 1995).

Grain Formation in Supernova Ejecta

Elemental Compositions in Supernova Ejecta

Stars born with more than 8-9 solar masses are short-lived (up to 30 million years, Heger et al. 2003, Woosley et al. 2002, Meynet 2015). Massive stars evolve very quickly to the red supergiant (RSG) and/or blue supergiant (BSG) stage where they lose mass in stellar winds before exploding as core-collapse supernovae and releasing most of their mass containing newly created elements (Smith, 2014). Supernovae leave behind a neutron star of about 1.34 $M_\odot$ and 20 km in diameter (black hole formation would occur from rare hypernovae of supermassive, 100+ $M_\odot$ stars).

The pre-explosion stellar winds of supergiants contain changes in C, N, and O abundances similar to those seen in AGB stars, but the yields in C, N, and O can vary considerably. The *s*-process element production is weak and limited to lighter elements such as Sr, Y, Zr; hence it is called the "weak *s* process" in massive stars versus the "main *s*-process" in low and intermediate mass stars (see Lugaro et al., this volume).

Table 4. Supernova nucleosynthesis summary

Major Isotope Burning, "Fuel"	Major products, "Ashes"	Where: When
^{1}H via H chain	H-burning ashes = ^{4}He	Core: Main sequence
	He zone (H-poor)	Shell: RGB, AGB, RSG
^{1}H via H chain and CNO cycle	H-burning ashes = ^{4}He	Core: Main sequence
	He/N zone (H-poor)	Shell: RGB, AGB, RSG
^{4}He	He-burning ashes = ^{12}C, ^{16}O	Core: Horizontal branch
	He/C zone (C>>O, H, He-poor[1]),	Shell: AGB, RSG
	O/C zone (O>> C, H, He-poor)	Explosive He burning
^{12}C	^{12}C-burning ashes = ^{16}O, ^{20}Ne, ^{23}Na, ^{24}Mg	Core & shell: RSG (>9 Msun)
	O/Ne zone (H, He, N-poor)	Explosive C burning
^{20}Ne	^{20}Ne-buring ashes = ^{16}O, ^{24}Mg	Core & shell: RSG (>9 Msun)
	O/Mg zone (H, He, N-poor)	Explosive Ne burning
^{16}O	^{16}O burning ashes = ^{28}Si, ^{32}S	Core & shell: RSG (> 9 Msun)
	Si/S zone (H, He, N, C, O, Mg-poor)	Explosive O burning
^{28}Si	^{28}Si burning ashes = ^{56}Ni, ^{56}Fe	Explosive Si burning[2]
	Ni zone	

1. Helium is still abundant (see Rauscher et al. 2002). 2. Si also burns before the explosion at 1.5 – 2.2 x 10^{9}K.

The elemental abundances in the explosion ejecta of supernova vary considerably from solar composition and are dominated by nucleosynthesis of alpha elements (e.g., O, Ne, Si, Ca, S, Ar, Fe) and others in the mass range up to iron. In massive stars, core burning does not stop with He-core burning. Shortly before core collapse and explosion, nucleosynthesis proceeds within "shells" or "zones" within the stars building heavier elements up to Fe in rapid sequence inwards, as illustrated in Table 4. The elemental and isotopic yields for these zones are derived from nucleosynthetic network computations for different stellar masses taking the complex physical conditions during evolution into account (see chapter by Brad Meyer, this volume; and Meyer et al. 1995, Woosley and Weaver 1995, Rauscher et al.

2002, Maeda and Nomoto 2003, Heger et al. 2003, den Hartogh et al. 2022). The products ("ashes") of nuclear burning provide the "fuel" for the next burning stage, e.g., burning of ^{12}C produces ^{16}O and ^{20}Ne making the O/Ne zone. Subsequently the ^{20}Ne and ^{16}O are burned to make heavier ^{24}Mg and ^{28}Si. Although C, N, O, Ne, Mg and Si are produced, the gradually processing also depletes H, He, N, C, O, S and Si in the resulting zones. These (time and initial mass-dependent) changes in bulk and zone compositions have consequences for the chemistry which is heavily influenced by H, C, O but also N and S in solar composition (see Table 5).

The comparison of the model isotopic compositions of supernova zones with those measured in presolar grains shows that less than 10% of the known presolar grains originated in supernovae. This includes reduced (SiC, graphite) and oxidized grains (e.g., Al_2O_3, spinel) as shown in Table 6. In order to obtain agreement of different isotope systems (C, O, Al, Mg, Si) mixing of material from different SN zones is often invoked (e.g., Travaglio et al. 1999). Mixing is also needed to match the elemental composition (in particular, C/O ratio) that gives the necessary redox conditions for grain stability, e.g., C/O > 1 is needed for graphite and SiC grains (see the discussion of Ebel and Grossman (2001) below).

Table 5. Supernova stratigraphy and chemistry

Supernova Stratigraphy	Elemental Composition compared to Solar	Effects on Chemistry
Outer-most Envelope	Solar-like	Solar-type condensates.
He zone	Solar-like He-rich H-poor	Increase in metallicity (X/H-ratio) causes higher condensation temperatures. Higher oxidation state from higher H_2O/H_2 Solar-type condensates.
He/N zone	Solar-like He, N-rich H-poor	As in He zone, high metallicity solar-like condensates. Increased stability of N-bearing gases and nitrides (TiN, AlN) under certain total pressures.
He/C zone	Solar-like, N, C-rich, He gradually depleted H-poor	As in He/N zone. High metallicity. C/O > 1 with C-dominated chemistry.
O/C zone	Solar-like N, C, O-rich He, H-poor	As in He/C zone. High metallicity. O>>C; C/O < 1, O-dominated chemistry.
O/Ne zone	O, Ne, Na, Mg rich H, He, N-poor	O-dominated chemistry.
O/Mg zone	O, Mg-rich H, He, N, Ne-poor	As in O/Ne zone.
Si/S zone	Si, S-rich H, He, N, Ne, C, O, Mg-poor	Sulfide dominated chemistry. Condensates: Silicides
Ni zone	Fe, Ni-rich	Atomic metal dominated gas. Condensates: Metal alloys, titanides, silicides

	H, He, N, C, O, Mg, S, Si-poor

Astronomical observations of dust from supernova are sparse, but many presolar grains from type II supernovae are known (e.g., the review by Hoppe et al. 2022). Dust formation in the aftermath of Type II supernovae is detectable through infrared emission from heated dust, e.g., in SN 1987A and more recently in SN 2003gd, SN 2005ip, and SN 2012aw (e.g., Matsuura et al. 2011, Gall et al. 2014). Observations of supernova remnants such as Cassiopeia A (Cas A; e.g., Hwang and Laming 2012) indicate that the ejecta are heterogeneous. Areas enriched in e.g., O, Si, S, and Fe are observed which could point towards more or less "pristine" SN zone composition. The findings of heterogeneous ejecta are in line with results for presolar supernova grains that call for mixing of supernova zones to match the chemical and isotopic compositions. Dust observations in SN ejecta and supernova remnant (SNR) are difficult and it is suspected that supernova dust grains are smaller than dust in AGB shells, which could make them harder to detect. Several dust minerals such as Al_2O_3, Mg_2SiO_4, $MgSiO_3$, FeS, carbon, SiC, and Fe_3O_4 are detected and inferred by matching grain emissions to spectral energy distributions (e.g., Rho et al. 2018, Sarangi et al. 2018).

Supernovae should be prolific dust producers given the production of large amounts of condensible elements, but detection of dust also depends on dust survival and escape to the interstellar medium from the shock-intense supernova ejecta. Slavin et al. (2020) followed the evolution of dust with hydrodynamical calculations. Large grains condensed in dense ejecta clumps within Cas A–like remnants will decouple from the gas after the clump is hit by the reverse shock. The remnant dust within the clump is destroyed by thermal and kinetic sputtering and only larger silicate (~0.25 μm) and carbonaceous (~0.1 μm) grains may survive the passage into the interstellar medium and beyond.

Table 6. Some presolar mineral grains and sub-grains from nova and supernova

E	Abund.	Mineral	Host grain	Reference(s)
C	7.08×10^{6}	TiC[a]	SiC	Singerling et al 2021
			graphite	Croat et al. 2003a
		Ti(N,C)	SiC	Gyngard et al. 2018
		Fe carbide (most likely)	SiC	Hynes et al. 2011
		Fe_3C	SiC	Singerling et al. 2021
		SiC	graphite	Croat et al. 2010
		ZrC[a]	SiC	Singerling et al 2021
N	1.95×10^{6}	(Al,Mg)N	SiC	Gyngard et al. 2018
		Ti(N,C)	SiC	Gyngard et al. 2018
Mg	1.02×10^{6}	(Al,Mg)N	SiC	Gyngard et al. 2018
		$MgSiO_3$	itself	Nguyen et al. 2016
Si	1.00×10^{6}	SiC	graphite	Croat et al. 2010

		FeSi	SiC	Singerling et al. 2021
		SiO_2	itself	Haenecour et al. 2013
		$MgSiO_3$	itself	Nguyen et al. 2016
		$(Mg_{0.83}Fe_{0.17})_2SiO_4$	itself	Messenger et al. 2005
Fe	8.38×10^5	Fe metal	graphite	Croat et al. 2002, 2003a,b
		Fe metal	SiC	Hynes et al. 2006
		Fe metal[b]	SiC	Singerling et al 2021
		FeNi alloys of variable composition	SiC	Gyngard et al. 2018
		FeNi alloys, kamacite (low Ni) & taenite (high Ni)	graphite	Croat et al. 2002, 2003a,b
		Fe carbide (most likely)	SiC	Hynes et al. 2011
		Fe_3C	SiC	Singerling et al. 2021
		FeSi	SiC	Singerling et al. 2021
		Pyrrhotite – like Fe sulfide (Fe 76±8 %, S 24±2 %, atom % values)	graphite	Haenecour et al. 2016
S	4.45×10^5	CaS (oldhamite)	SiC	Hynes et al. 2011
		Pyrrhotite – like Fe sulfide (Fe 76±8 %, S 24±2 %, atom % values)	graphite	Haenecour et al. 2016
Al	8.41×10^4	(Al,Mg)N	SiC	Gyngard et al. 2018
Ca	6.29×10^4	CaS (oldhamite)	SiC	Hynes et al. 2011
Ni	4.78×10^4	FeNi alloys, kamacite & taenite	graphite	Croat et al. 2002, 2003a,b
		Ni metal[c]	SiC	Singerling et al 2021
		(Fe,Ni) silicides	SiC	Hynes et al. 2010
Ti	2.42×10^3	TiC[a]	SiC	Singerling et al. 2021
			graphite	Croat et al. 2003a
		Ti(N,C)	SiC	Gyngard et al. 2018
		ZrC[a]	SiC	Singerling et al. 2021
Zr	10.9	ZrC[a]	SiC	Singerling et al. 2021
W	0.144	$W_{100-x}Fe_x$ (4<x<22) alloy	graphite	Croat et al. 2013

[a]The TiC and ZrC sub-grains are solid solutions with variable Ti/Zr ratios. See Table 3 in Singerling et al. 2021. [b]Singerling et al. 2021 report variable Fe/Ti ratios but no Ni in the Fe metal grains they studied. [c]Singerling et al. 2021 report Ni/Ti of 20±10 and Fe/Ni of 0.29±0.06 in a Ni metal sub-grain.

Dust grains from supernovae.

The elemental zone compositions from nucleosynthetic network computations and hydrodynamic codes (referenced above) are used as starting points to model dust formation with thermochemical and/or kinetic condensation codes (e.g., Lattimer et al. 1978, Kozasa et al. 1989, Ebel & Grossman 2001, Todini & Ferrara 2001, Nozawa et al. 2003, Bianchi and Schneider 2007, Cherchneff and Dwek 2010). The early work by Lattimer et al. (1978) is still among the most detailed computations about the condensates expected for individual supernova shells. However, far more refined abundance tables as well as thermochemical tools are available now than in 1978 when Lattimer et al. (1978) did their study.

The work by Ebel & Grossman (2001) addresses an important question of whether or not reduced condensates can form at C/O < 1 if formation of CO and other gaseous molecules are suppressed for some reason, as suggested by Clayton et al. (1999). Ebel & Grossman (2001) found TiC stable in the innermost supernova shells where the mass balance

$$[Ti + Si] \gg [C + O]$$

was satisfied, but neither SiC nor graphite was stable. However, neither carbides nor graphite are stable in the intermediate O-rich shells lying between the inner heavy element rich shells and the outer C-rich shells where reduced mineralogy is stable. Although graphite could be produced in O-rich supernova shells if formation of molecular gases were suppressed, it is accompanied by silica SiO_2, which is not found with presolar graphite in meteorites. The results of Ebel & Grossman (2001) reinforce earlier conclusions that at complete chemical equilibrium carbides and graphite are stable condensates *only* at C/O >1 (e.g., Gilman 1969, Larimer 1975, Larimer & Bartholomay 1979).

Models of grain formation in SN using chemical kinetics and nucleation theory can make predictions about when, where, and what type of grains appear in the ejecta. These models are dependent on the assumed overall conditions (mass of initial star, mass-cut, explosion parameters, nucleosynthetic yields of individual zones and mixing parameters) but also on the condensate material properties used in the models (thermodynamic data, surface energies, sticking probabilities, reaction rate constants, assumed super-saturation ratios,) which often involve estimates. Equilibrium models are path-independent and only require thermodynamic data for gases and condensates (e.g., Gibbs free energies), which are available for many gases and solids of major and trace elements from experimental measurements or quantum mechanical calculations. In contrast, complex dust formation models using kinetic networks and nucleation constraints are often limited to major element-bearing minerals, e.g., Al_2O_3, MgO, SiO_2, Mg_2SiO_4, $MgSiO_3$, FeS, carbon, SiC, Fe_3O_4, TiO_2, and TiC (Kozasa et al. 1989, Todini & Ferrara 2001, Nozawa et al. 2003, Cherchneff & Dwek 2010).

Physical Setting in Supernova Ejecta

Not much is known about the actual temperature and density (pressure) structure in supernova ejecta where grains form because these quantities are time dependent. The ejecta environment after core-collapse is influenced by the SN explosion blast wave slamming and compressing the shell created by the pre-SN (RSG, BSG or WR) star into the ambient ISM causing shock waves and Rayleigh-Taylor instabilities as well as the reverse shock (e.g., Kurfürst and Krtička 2019). Supersonic ejection flows, turbulent mixing, and radioactive heating will superimpose additional controls on temperature, density and total pressure and thus on chemistry. Early work on condensation for SN ejecta by Lattimer et al. (1978) or e.g., Kozasa et al. (1989) took some of these variables into account when deriving estimates for the time and spatially dependent temperature and pressure conditions in the ejecta for their condensation computations. One key result is that total pressures vary over twelve orders of magnitude in the cooling ejecta. Thus, condensate stability over a wide range in temperature and total pressure needs to be computed and evaluated, which is easily done for a constant bulk elemental composition.

Kozasa et al. (1989) used approximations for the density (D) and temperature (T) structure at given expansion time (t) after explosion:

$D_{gas}(t) = D_{photo}\ (t_{photo}/t)^3$

$T_{gas}(t) = [T_{photo}(t_{photo})/t]^{\wedge(3(gamma-1))}$

Where the superscripts "photo" stands for the photospheric condition (t_{photo} is the time at which the photosphere has density D_{photo} and temperature T_{photo}.). Gamma is the adiabatic index (ratio of constant volume and constant pressure heat capacity, C_V/C_P).

Models by Cherchneff & Dwek (2010) invoke cluster growth of metal grains (Fe,Mg,Si), metal oxides (SiO_2, MgO, FeO, Al_2O_3), metal sulfides (FeS, MgS), silicates (forsterite Mg_2SiO_4 and fayalite Fe_2SiO_4), silicon carbide (SiC), and amorphous carbon dust. For simplicity, they excluded possible formation of magnesium silicide Mg_2Si and pyroxenes (enstatite $MgSiO_3$ and ferrosilite $FeSiO_3$ solid solutions). This may limit the applicability of the results because pyroxenes are widespread in chondritic meteorites and interplanetary dust particles, which are samples of nebular material, and are well-known sinks for SiO (gas). The formation of enstatite proceeds by reaction of forsterite via the net reaction:

$$Mg_2SiO_4\ (forsterite) + SiO\ (g) + H_2O\ (g) = 2\ MgSiO_3\ (enstatite) + H_2\ (g)$$

If pyroxenes are ignored, SiO forms silica (SiO_2) instead, or in an extreme case, native Si metal may condense, as predicted in Cherchneff & Dwek (2010).

An important issue often raised is whether the forsterite to enstatite reaction can proceed towards equilibrium in a cooling gas. It requires that forsterite dust remains in equilibrium with the gas, which could be a problem if forsterite grains are expelled from hot regions by radiation pressure into outer cooler regions where reactions are becoming very slow. Another issue is that grain temperatures could be higher than those of the surrounding gas from radiative heating. This affects solid-gas reactions. If grains are too hot in a warm gas, the condensation reaction, e.g., for enstatite above, shifts towards the left side to favor SiO(g) retention in the gas from equilibrium principles. On the other hand, a hot grain

in a cold gas may enable SiO (g) uptake because the kinetic inhibition through the reaction activation energy is lowered.

Acknowledgments

We thank Sachiko Amari for the invitation to contribute a chapter to this book and for many helpful discussions of presolar grain chemistry during the past 30+ years. Work supported by NSF AST- 2108172 and the McDonnell Center for the Space Sciences.

References

Abia, C., Hedrosa, R.P., Domínguez, I., Straniero, O., 2017. The puzzle of the CNO isotope ratios in asymptotic giant branch carbon stars. Astron. Astrophys. 599, A39 11 pp.

Adams, G.M., Lodders K., 2024. Effects of metallicity on graphite, TiC, and SiC condensation in carbon stars. Abstract No. 6198, 86th meeting of the Meteoritical Society, LPI Contribution No. 3036

Aller, L.A., 1963. *The Atmospheres of the Sun and Stars*, 2nd ed, Ronald Press, New York.

Belov, G.V., Iorish, V.S., Yungman, V.S., 1999. IVTANTHERMO for windows - database on thermodynamic properties and related software. CALPHAD 23, 173–180.

Bernatowicz, T.J., Cowsik, R., Gibbons, P.C., Lodders, K., Fegley, B., Amari, S., Lewis, R. S., 1996. Constraints on stellar grain formation from presolar graphite in the Murchison meteorite. Astrophys. J. 472, 760-782.

Bernatowicz, T.J., Akande, O.W., Croat, T.K., Cowsik, R., 2005. Constraints on grain formation around carbon stars from laboratory studies of presolar graphite. Astrophys. J. 631, 988-1000.

Bianchi, S., Schneider, R., 2007. Dust formation and survival in supernova ejecta. Mon. Not. R. Astron. Soc. 378, 973–982, https://doi.org/10.1111/j.1365-2966.2007.11829.x

Blander, M., Fuchs, L.H., Horowitz, C., Land, R., 1980. Primordial refractory metal particles in the Allende meteorite. Geochim. Cosmochim. Acta 44, 217-223.

Bose M., Floss C., Stadermann F.J., Stroud R.M. and Speck A.K. (2012) Circumstellar and interstellar material in the CO3 chondrite ALHA77307: An isotopic and elemental investigation. *Geochim. Cosmochim. Acta* 93, 77-101.

Boynton, W.V., 1975. Fractionation in the solar nebula: Condensation of yttrium and the rare earth elements. Geochim. Cosmochim. Acta 37, 1119–1140.

Bruce, R.H., 1965. Aspects of the surface energy of ceramics I – Calculation of surface free energies in Science of Ceramics, G.H. Stewart, Ed., vol. 2, pp. 359-381.

Busemann, H., Nguyen, A. N., Cody, G. D., Hoppe, P., Kilcoyne, A. L. D., Stroud, R. M., Zega, T. J. and Nittler, L. R. (2009) Ultra-primitive interplanetary dust particles from the comet 26P/Grigg-Skjellerup dust stream collection. *Earth Planet. Sci. Lett.* 288, 44–57.

Lodders, K., & Fegley, B. (2025). Mineral condensation in stellar outflows. In *Presolar Grains in Extra-Terrestrial Materials: Probing Stars with Stardust* (pp. 539-583). Elsevier. https://doi.org/10.1016/B978-0-12-821830-3.00002-4. Revised 29 August 2024. Preprint.

Cameron, A.G.W., Fegley, M.B., 1982. Nucleation and condensation in the primitive solar nebula. Icarus 52, 1-13.

Cherchneff, I., Dwek, E., 2010. The chemistry of population III supernova ejecta. II. The nucleation of molecular clusters as a diagnostic for dust in the early universe. Astrophys. J. 713, 1-24.

Chigai, T., Yamamoto, T., Kozasa, T., 2002. Heterogeneous condensation of presolar titanium carbide core-graphite mantle spherules. Meteorit. Planet. Sci. 37, 1937–1951.

Clayton, D.D., Liu, W., Dalgarno, A., 1999. Condensation of carbon in radioactive supernova gas. Science 283, 1290-1292.

Croat T.K. (2007) Rutile found within presolar graphites from Murchison. *Meteorit. Planet. Sci.* 42, A34.

Croat T.K., Bernatowicz T.J., Amari S., Messenger S. and Stadermann F.J. (2002) Metallic iron condensed onto titanium carbides within supernova graphites. *Meteorit. Planet. Sci.* 37, A39.

Croat K., Bernatowicz T., Stadermann F.J., Messenger S. and Amari S. (2002) Coordinated isotopic and TEM studies of a supernova graphite. *Lunar Planet. Sci.* XXXIII, Abstract #1315.

Croat, T.K., Bernatowicz, T., Amari, S., Messenger, S., Stadermann, F.J., 2003a. Structural, chemical, and isotopic microanalytical investigations of graphite from supernovae. Geochim. Cosmochim. Acta 67, 4705-4725.

Croat T.K., Bernatowicz T., Stadermann F.J., Messenger S. and Amari S. (2003b) TEM study of internal crystals in supernova graphites. *Lunar Planet. Sci.* XXXIV, Abstract #1470.

Croat T.K., Stadermann F.J., Zinner E. and Bernatowicz T.J. (2004) Coordinated isotopic and TEM studies of presolar graphites from Murchison. *Lunar Planet. Sci.* XXXV, Abstract #1353.

Croat T.K., Stadermann F.J. and Bernatowicz T.J. (2005) Presolar graphite from AGB stars: Microstructure and s-process enrichment. *Astrophys. J.* 631, 976-987.

Croat T.K., Stadermann F. and Bernatowicz T. (2008) Correlated isotopic and microstructural studies of turbostratic presolar graphites from the Murchison meteorite. *Meteorit. Planet. Sci.* 43, 1497-1516.

Croat T.K., Stadermann F.J. and Bernatowicz T.J. (2010) Unusual 29,30Si-rich SiCs of massive star origin found within graphites from the Murchison meteorite. *Astron. J.* 139, 2159-2169.

Croat T.K., Berg T., Bernatowicz T.J. and Jadhav M. (2013a) Refractory metal nuggets within presolar graphite: First condensates from a circumstellar environment. *Meteorit. Planet. Sci.* 48, 686-699.

Croat T.K., Amari S. and Bernatowicz T.J. (2013b) Isotopic and microstructural studies of low density graphites with extreme C anomalies. *Lunar & Planet. Sci.* 44, abstract #2415.

den Hartogh, J., Petö, M.K., Lawson, T., Sieverding, A., Brinkman, H., Pignatari, M., Lugaro, M., 2022. Comparison between core collapse supernova nucleosynthesis and meteoritic stardust grains: Investigating magnesium, aluminum, and chromium. Astrophys. J. 927:220 (24 pp).

Duga, J.J., 1969. Surface energy of ceramic materials. DCIC report 69-2 Battelle Memorial Institute.

Lodders, K., & Fegley, B. (2025). Mineral condensation in stellar outflows. In *Presolar Grains in Extra-Terrestrial Materials: Probing Stars with Stardust* (pp. 539-583). Elsevier. https://doi.org/10.1016/B978-0-12-821830-3.00002-4. Revised 29 August 2024. Preprint.

Ebel, D.S., 2000. Variations on solar condensation: Sources of interstellar dust nuclei. J. Geophys. Res. 105, 10363–10370.

Ebel, D.S., 2006. Condensation of Rocky Material in Astrophysical Environments. In Meteorites and the Early Solar System II (D. S. Lauretta and H. Y. McSween Jr., eds.), Univ. of Arizona, Tucson, pp 253-277.

Ebel, D.S. 2021 Condensation calculations in planetary science and cosmochemistry. Oxford Research Encyclopedia of Planetary Science, doi.org/10.1093/acrefore/9780190647926.013.201

Ebel, D. S., Grossman, L., 2000. Condensation in dust-enriched systems. Geochim. Cosmochim. Acta 64, 339–366.

Ebel, D.S., Grossman L. 2001 Condensation from supernova gas made of free atoms. Geochim. Cosmochim. Acta 65, 469–477.

Elliott, J.F., Gleiser, M., Ramakrishna, V., 1963, Thermochemistry for Steelmaking, vol II, pp. 654-658, Addison-Wesley, Reading, MA.

Fegley, B., 2013. Practical Chemical Thermodynamics for Geoscientists, Academic Press, Waltham, MA.

Fegley, B., Lewis, J.S., 1980. Volatile element chemistry in the solar nebula: Na, K, F, Cl, Br, and P. Icarus 41, 439-455.

Fegley, B., Lodders, K., 1994. Chemical models of the deep atmospheres of Jupiter and Saturn. Icarus 110, 117-154.

Fegley, B., Palme, H., 1985. Evidence for oxidizing conditions in the solar nebula from Mo and W depletions in refractory inclusions in carbonaceous chondrites. Earth Planet. Sci. Lett. 72, 311–326.

Fegley, B., Prinn, R.G., 1985. Equilibrium and nonequilibrium chemistry of Saturn's atmosphere: Implications for the observability of PH_3, N_2, CO, and GeH_4. Astrophys. J. 299, 1067-1078.

Fegley, B., Schaefer, L., 2010. Cosmochemistry, in Principles and Perspectives in Cosmochemistry: Lecture Notes of the Kodai School on Synthesis of Elements in Stars, pp. 347-377, eds. A. Goswami, B.E. Reddy, Springer.

Fegley, B., Lodders, K., Jacobson, N.S., 2023. Chemical Equilibrium Calculations for Bulk Silicate Earth Material at High Temperatures. Geochemistry (formerly Chemie der Erde) 83, 125961 (35 pp)

Ferrarotti, A.S., Gail, H.-P., 2001. Mineral formation in stellar winds II. Effects of Mg/Si abundance variations on dust composition in AGB stars. Astron. Astrophys. 371, 133-151.

Ferrarotti, A.S., Gail, H.-P., 2006. Composition and quantities of dust produced by AGB-stars and returned to the interstellar medium. Astron. Astrophys. 447, 553-576.

Floss C. and Stadermann F. (2009) Auger Nanoprobe analysis of presolar ferromagnesian silicate grains from primitive CR chondrites QUE 99177 and MET 00426. *Geochim. Cosmochim. Acta* 73, 2415-2440.

Lodders, K., & Fegley, B. (2025). Mineral condensation in stellar outflows. In *Presolar Grains in Extra-Terrestrial Materials: Probing Stars with Stardust* (pp. 539-583). Elsevier. https://doi.org/10.1016/B978-0-12-821830-3.00002-4. Revised 29 August 2024. Preprint.

Frost, C.A., Cannon, R.C., Lattanzio, J.C., Wood, P.R., Forestini, M., 1998. The brightest carbon stars. Astron. Astrophys. 332, L17–L20. doi:10.48550/arXiv.astro-ph/9710054

Gall, C., Hjorth, J., & Andersen, A. C. (2014). The dust-scattered X-ray halo around the GRB 031203 optical supernova. Nature, 511(7509), 326-328.

Gilman, R.C., 1969. On the composition of circumstellar grains. Astrophys. J. 155, L185-L187.

Grossman, L., 1980. Refractory inclusions in the Allende meteorite. Annu. Rev. Earth Planet. Sci. 8, 559-608.

Grossman, L., Larimer J.W., 1974. Early chemical history of the solar system. Rev. Geophys. Space Phys. 12, 71–101.

Grossman, L., 1972. Condensation in the primitive solar nebula. Geochim. Cosmochim. Acta, 36, 597–619.

Gyngard F., Jadhav M., Nittler L.R., Stroud R.M. and Zinner E. (2018) Bonanza: An extremely large dust grain from a supernova. *Geochim. Cosmochim. Acta* 221, 60-86.

Haenecour P., Zhao X., Floss C., Lin Y. and Zinner E. (2013) First laboratory observation of silica grains from core collapse supernovae. *Astrophys. J. Lett.* 768, L17 (15pp).

Haenecour, P., Floss, C., Jose, J., Amari, S., Lodders, K., Jadhav, M., Wang, A., Gyngard, F., 2016. Coordinated Analysis of Two Graphite Grains from the CO3.0 LAP 031117 Meteorite: First identification of a CO nova graphite and a presolar iron sulfide subgrain. Astrophys. J. 825, 88 (9 pp)

Haenecour, P., Howe, J.Y., Zega, T.J., Amari, S., Lodders, K., Jose, J., Kaji, K., Sunaoshi, T., Muto, A., 2019. Laboratory evidence for co-condensed oxygen- and carbon-rich meteoritic stardust from nova outbursts. Nature Astronomy, 3, 626-630.

Harkins, W.D., 1942. Energy relations of the surface of solids I. Surface energy of the diamond. J. Chem. Phys. 10, 268-272.

Heger, A., Fryer, C.L., Woosley, S.E., Langer, N., Hartmann, D.H., 2003. How massive single stars end their life. Astrophys. J. 591, 288-300.

Herwig, F., 2013. Evolution of Solar and Intermediate-Mass Stars, in: Planets, Stars, and Stellar Systems, volume 4: Stellar Structure and Evolution, eds. T.D. Oswalt (editor in chief), M.A. Barstow (volume editor), chapter 8, pp. Springer Dordrecht, The Netherlands, pp. 397-446.

Hirschfelder, J.O., Curtiss, C.F., Bird, R.B., 1964. Molecular Theory of Gases and Liquids, Corrected Printing with Notes Added. John Wiley, NY.

Hoppe, P., Leitner, J., Kodolanyi, J., Borrmann, S., Jones, A.P., 2022. Dust from supernovae and their progenitors in the solar nebula. Nature Astronomy 6, 1027–1034.

Hwang, U., Laming, J.M., 2012. A Chandra X-ray Survey of Ejecta in the Cassiopeia A. Astrophys. J. 746, 130 (18 pp)

Lodders, K., & Fegley, B. (2025). Mineral condensation in stellar outflows. In *Presolar Grains in Extra-Terrestrial Materials: Probing Stars with Stardust* (pp. 539-583). Elsevier. https://doi.org/10.1016/B978-0-12-821830-3.00002-4. Revised 29 August 2024. Preprint.

Hynes K.M. and Croat T.K. (2007) Silicon carbide subgrains in presolar graphite from Murchison. *Meteorit. Planet. Sci.* 42, A72.

Hynes K.M., Croat T.K., Amari S., Mertz A.F. and Bernatowicz T.J. (2006) A transmission electron microscope study of internal subgrains in SiC-X grains. *Meteorit. Planet. Sci.* 41, A83.

Hynes K.M., Croat T.K., Amari S., Mertz A.F. and Bernatowicz T.J. (2010) Structual and isotopic microanalysis of presolar SiC from supernovae. Meteorit. *Planet. Sci.* 45, 596-614.

Hynes K.M., Amari S., Bernatowicz T.J., Lebsack E., Gyngard F. and Nittler L.R. (2011) Combined TEM and NanoSIMS analysis of subgrains in a SiC AB grain. *Lunar Planet Sci.* XLII, Abstract #2332.

Jose, J., Hernanz, M., Amari, S., Lodders, K., Zinner, E., 2004. The imprint of nova nucleosynthesis in presolar grains. Astrophys. J. 612, 414-428.

Jose, J. and Hernanz, M., 2007. The origin of presolar nova grains. Meteoritics & Planetary Science, 42(7-8), pp.1135-1143.

Kornacki, A.S., Fegley, B., 1986. The abundance and relative volatility of refractory trace elements. Earth Planet. Sci. Lett. 79, 217–234.

Kozasa, T., Hasegawa, H., Nomoto, K., 1989. Formation of dust grains in the ejecta of SN 1987A. Astrophys. J. 344, 325-331.

Kurfürst, P., Krtička, J., 2019. Modeling of interactions between supernovae ejecta and aspherical circumstellar environments, Astron. Astrophys. 625, A24 (16pp).

Lach, F., Röpke, F.K., Seitenzahl, I.R., Coté, B., Gronow, S., Ruiter, A.J., 2020. Nucleosynthesis imprints from different Type Ia supernova explosion scenarios and implications for galactic chemical evolution. Astron. Astrophys. 644, A118 (15pp).

Larimer, J. W., 1967. Chemical fractionation in meteorites, I. Condensation of the elements. Geochim. Cosmochim. Acta, 31, 1215–1238.

Larimer, J.W., 1973. Chemical fractionations in meteorites – VII. Cosmothermometry and cosmobarometry. Geochim. Cosmochim. Acta 37, 1603-1623.

Larimer, J.W., 1975. The effect of C/O ratio on the condensation of planetary material. Geochim. Cosmochim. Acta 39, 389–392.

Larimer, J.W., Anders, E., 1967. Chemical fractionations in meteorites: II. Abundance patterns and their interpretation. Geochim. Cosmochim. Acta 31, 1239–1270.

Larimer, J.W., Bartholomay, H.A., 1979. The role of carbon and oxygen in cosmic gases: Some applications to the chemistry and mineralogy of enstatite chondrites. Geochim. Cosmochim. Acta 43, 1455–1466.

Lattimer, J.M., Schramm, D.N., Grossman, L., 1978. Condensation in supernova ejecta and isotopic anomalies in meteorites. Astrophys. J. 219, 230–249.

Lodders, K., & Fegley, B. (2025). Mineral condensation in stellar outflows. In *Presolar Grains in Extra-Terrestrial Materials: Probing Stars with Stardust* (pp. 539-583). Elsevier. https://doi.org/10.1016/B978-0-12-821830-3.00002-4. Revised 29 August 2024. Preprint.

Livey, D.T., Murray, P., 1956. Surface energies of solid oxides and carbides. J. Am. Ceram. Soc. 39, 363-372.

Lodders, K., 1999. Revised thermochemical properties of phosphinidene (PH), phosphine (PH_3), phosphorus nitride (PN), and magnesium phosphate ($Mg_3P_2O_8$). J. Phys. Chem. Ref. Data 28, 1705-1712.

Lodders, K., 2002. Titanium and vanadium chemistry in low-mass dwarf stars Astrophys. J. 577, 974-985.

Lodders, K., 2003. Solar system abundances and condensation temperatures of the elements. Astrophys. J. 591, 1220–1247.

Lodders, K., 2004. Revised and updated thermochemical properties of the gases mercapto (HS), disulfur monoxide (S_2O), thiazyl (NS), and thioxophosphino (PS). J. Phys. Chem. Ref. Data 33, 357-367.

Lodders, K., 2006. They came from deep in the supernova: The origin of TiC and metal-subgrains in presolar graphite grains. Astrophys. J. 647, L37-L40.

Lodders, K., 2008. Circumstellar chemistry and dust from dead stars in meteorites. In Chemical Evolution I: Chemical Evolution Across Space and Time, L. Zaikovski, J. M. Friedrich (eds.) Amer. Chem. Soc. Symp. Ser. 981, Washington D.C.

Lodders, K., 2020. Solar elemental abundances. In The Oxford Research Encyclopedia of Planetary Sciences. doi.org/10.1093/acrefore/9780190647926.013.145

Lodders, K., Amari, S., 2005. Presolar grains from meteorites: Remnants from the early time of the solar system. Chem. Erde 65, 93-166.

Lodders, K., Fegley, B., 1993. Lanthanide and actinide chemistry at high C/O ratios in the solar nebula. Earth Planet. Sci. Lett. 117, 125–145.

Lodders, K., Fegley, B., 1995. The origin of circumstellar silicon carbide grains found in meteorites. Meteoritics 30, 661-678.

Lodders, K., Fegley, B., 1997. Condensation chemistry of carbon stars. In Astrophysical Implications of the Laboratory Study of Presolar Materials (T. J. Bernatowicz and E. Zinner, eds.), pp. 391–424. AIP Conference Proceedings 402, American Institute of Physics, New York.

Lodders, K., Fegley, B., 1999. Condensation chemistry of circumstellar grains. In Asymptotic Giant Branch Stars, T. Le Bertre, A. Lebre, C. Waelkens, eds., pp. 279-291, IAU Symposium 191, Astron Soc Pacific.

Lodders, K., Fegley, B., 2002. Atmospheric chemistry in giant planets, brown dwarfs, and low-mass dwarf stars. Icarus 155, 393-424.

Lodders, K. and Fegley Jr, B., 2023. Solar system abundances and condensation temperatures of the halogens fluorine, chlorine, bromine, and iodine. Geochemistry, 83(1), p.125957.

Maeda, K., Nomoto, K., 2003. Bipolar supernova explosions: Nucleosynthesis and implications for abundances in extremely metal-poor stars. Astrophys. J. 598, 1163-1200.

Lodders, K., & Fegley, B. (2025). Mineral condensation in stellar outflows. In *Presolar Grains in Extra-Terrestrial Materials: Probing Stars with Stardust* (pp. 539-583). Elsevier. https://doi.org/10.1016/B978-0-12-821830-3.00002-4. Revised 29 August 2024. Preprint.

Matsuura, M., Dwek, E., Meixner, M., et al., 2011. Warm dust and polycyclic aromatic hydrocarbon emission in 19 nearby galaxies. Mon. Not. R. Astron. Soc. 418(1), 249-266.

Messenger, S., Keller, L. P., Stadermann, F. J., Walker, R. M. and Zinner, E. (2003) Samples of stars beyond the solar system: silicate grains in interplanetary dust. *Science* 300, 105–108.

Messenger, S., Keller, L. P. and Lauretta, D. S. (2005) Supernova olivine from cometary dust. *Science* 309, 737–741.

Meyer, B.S., Weaver, T.A., Woosley, S.E., 1995. Isotope source table for a 25 $M_\odot$ supernova. Meteoritics 30, 325-334.

Meynet, G., Kudritzki, R.-P., Georgy, C., 2015. The flux-weighted gravity-luminosity relationship of blue supergiant stars as a constraint for stellar evolution. Astron. Astrophys. 581, A36 (15pp).

Nittler, L., Alexander, C.M.O'D., Liu, N., Wang, J. 2018. Extremely ^{54}Cr- and ^{50}Ti-rich Presolar Oxide Grains in a Primitive Meteorite: Formation in Rare Types of Supernovae and Implications for the Astrophysical Context of Solar System Birth. Astrophys. J. 856, L24 (7pp).

Nguyen A.N., Nittler L.R., Stadermann F.J., Stroud R.M. and Alexander C.M.O'D. (2010) Coordinated analyses of presolar grains in the Allan Hills 77307 and Queen Elizabeth Range 99177 meteorites. *Astrophys. J.* 719, 166-189.

Nguyen, A. N., Keller, L. P., Rahman, Z. and Messenger, S. (2013) Crystal structure and chemical composition of a presolar silicate from the Queen Elizabeth Range 99177 meteorite. *Lunar Planet. Sci.* XLIV, #2853.

Nguyen A.N., Keller L.P. and Messenger S. (2016) Mineralogy of presolar silicate and oxide grains of diverse stellar origins. *Astrophys. J.* 818:51, (17pp).

Nguyen A.N., Keller L.P., Brownlee D.E. and Joswiak D.J. (2023) Mineralogy of presolar grains of varied stellar origins in giant cluster IDP U2-20GCA. *Lunar & Planet. Sci.* 54, Abstract #2535.

Nomoto, K., Iwamoto, K., Nakasato, N., Thielemann, F.-K., Brachwitz, F., Tsujimoto, T., Kubo, Y., et al., 1997. Nucleosynthesis in type Ia supernovae. Nuclear Physics A 621, 467–476.

Nozawa, T., Kozasa, T., Umeda, H., Maeda, K., Nomoto, K. 2003. Dust in the Early Universe: Dust Formation in the Ejecta of Population III Supernovae. Astrophys. J. 598, 785-803.

Olofsson, H., 1997. The neutral envelopes around AGB and post-AGB objects, in Molecules in Astrophysics: Probes, Processes, (ed. E.F. van Dishoeck), IAU, pp. 457-468.

Palme, H., Fegley, B., 1990. High-temperature condensation of iron-rich olivine in the solar nebula. Earth Planet. Sci. Lett. 101, 180-195.

Palme, H., Wlotzka, F., 1976. A metal particle from a Ca, Al-rich inclusion from the meteorite Allende, and the condensation of refractory siderophile elements. Earth Planet. Sci. Lett. 33, 45-60.

Palme, H., Wlotzka, F., Nagel, K., El Goresy, A., 1982. An ultra-refractory inclusion from the Ornans carbonaceous chondrite. Earth Planet. Sci. Lett. 61, 1-12.

Lodders, K., & Fegley, B. (2025). Mineral condensation in stellar outflows. In *Presolar Grains in Extra-Terrestrial Materials: Probing Stars with Stardust* (pp. 539-583). Elsevier. https://doi.org/10.1016/B978-0-12-821830-3.00002-4. Revised 29 August 2024. Preprint.

Pitthan, E., Amarasinghe, V.P., Xu, C., Gustafsson, T., Stedile, F.C., Feldman, L.C., 2017. 4H-SiC surface energy tuning by nitrogen uptake. Appl. Surf. Sci. 402, 192-197.

Prinn, R.G., Barshay, S.S., 1977. Carbon monoxide on Jupiter and implications for atmospheric convection. Science 198, 1031-1034.

Prinn, R.G., Fegley, B., 1989. Solar nebula chemistry: Origin of planetary, satellite, and cometary volatiles. In Origin and Evolution of Planetary and Satellite Atmospheres, S. Atreya, J. Pollack, M.S. Matthews, eds. pp. 78-136, University of Arizona Press, Tucson, AZ.

Rauscher, T., Heger, A., Hoffmann, R.D., Woosley, S.E., 2002. Nucleosynthesis in massive stars with improved nuclear and stellar physics. Astrophys. J. 576, 323-348.

Rhee, S.K. 1972a. Critical surface energies of Al_2O_3 and graphite. J. Am. Ceram. Soc. 55, 300-303.

Rhee, S.K., 1972b. A method for determining surface energies of solids: temperature – variant contact angle method. Mat. Sci. Eng. 16, 45-51.

Rho, J., Gomez, H.L., Boogert, A., Smith, M.W.L., Lagage, P.O., Dowell, D., Clark, C J R., Peeters, E., Cami, J., 2018. A dust twin of Cas A: cool dust and 21 μm silicate dust feature in the supernova remnant G54.1+0.3. Mon. Not. R. Astron. Soc. 479, 5101–5123.

Robie, R.A., Hemingway, B.S., 1995. Thermodynamic properties of minerals and related substances at 298.15◦ K and 1 bar (105 Pascals) pressure and at higher temperatures. U.S. Geol. Surv. Bull. 2131.

Ruscic, B., Wagner, A.F., Harding, L.B., Asher, R.L., Feller, D., Dixon, D.A., Peterson, K.A., Song, Y., Qian, X., Ng, C.-Y., Liu, J., Chen, W., Schwenke, D.W., 2002. On the enthalpy of formation of hydroxyl radical and gas-phase bond dissociation energies of water and hydroxyl. J. Phys. Chem. A 106, 2727-2747.

Salpeter, E.E., 1974. Nucleation and growth of dust grains. Astrophys. J. 193, 579-584.

Sarangi, A., Matsuura, M., Micelotta, E.R., 2018. Dust in Supernovae and Supernova Remnants I: Formation Scenarios. Space Sci. Rev. 214, 63 (48pp). DOI: 10.1007/s11214-018-0492-7

Saxena, S.K., Eriksson, G., 1983a. High temperature phase equilibria in a solar -composition gas. Geochim. Cosmochim. Acta 47, 1865-1874.

Saxena, S.K., Eriksson, G., 1983b. Low- to medium-temperature phase equilibria in a gas of solar composition. Earth Planet. Sci. Lett. 65, 7-16.

Sears, D.W., 1978. Condensation and the composition of iron meteorites. Earth Planet. Sci. Lett. 41, 128-138.

Sedlmayr, E., Krüger, D., 1997. Formation of dust particles in cool stellar outflows. In Astrophysical Implications of the Laboratory Study of Presolar Materials (T. J. Bernatowicz and E. Zinner, eds.), pp. 425–450. AIP Conference Proceedings 402, American Institute of Physics, New York.

Sharp, C.M., Huebner, W.F., 1990. Molecular equilibrium with condensation. Astrophys. J. Suppl. 72, 417-431.

Lodders, K., & Fegley, B. (2025). Mineral condensation in stellar outflows. In *Presolar Grains in Extra-Terrestrial Materials: Probing Stars with Stardust* (pp. 539-583). Elsevier. https://doi.org/10.1016/B978-0-12-821830-3.00002-4. Revised 29 August 2024. Preprint.

Sharp, C.M., Wasserburg, G.J., 1995. Molecular equilibria and condensation temperatures in carbon-rich gases. Geochim. Cosmochim. Acta 59, 1633–1652.

Singerling S.A., Liu N., Nittler L.R., Alexander C.M.O'D. and Stroud R.M. (2021) TEM Analyses of Unusual Presolar Silicon Carbide: Insights into the Range of Circumstellar Dust Condensation Conditions. *Astrophys. J.* 913:90, (65pp).

Slavin, J.D., Dwek, E., Mac Low, M.M., Hill, A.S., 2020. The Dynamics, destruction, and survival of Supernova-formed Dust Grains. Astrophys. J. 902, 135 (12pp).

Smith, N. 2014. Mass Loss: Its Effect on the Evolution and Fate of High-Mass Stars. Annu. Rev, Astron. Astrophys. 52, 487–528. doi:10.1146/annurev-astro-081913-040025

Stroud R.M. and Bernatowicz T.J. (2005) Surface and internal structure of pristine presolar silicon carbide. *Lunar & Planet. Sci.* 36, abstract #2010.

Stroud, R. M., De Gregorio, B. T., Nittler, L. R. and Alexander, C. M. O'D. (2014) Comparative transmission electron microscopy studies of presolar silicate and oxide grains from the Dominion Range 08006 and Northwest Africa 5958 meteorites. *Lunar Planet. Sci.* XLV, #2806.

Symonds, R.B., Rose, W.I., Bluth, G.J.S., Gerlach, T.M., 1994. Volcanic-gas studies: Methods, results, and applications. In *Volatiles in Magmas* (M. R. Carroll and J. R. Holloway, Eds.), pp. 1–66. Mineral. Soc. Amer., Washington, D.C.

Takigawa A., Stroud R. M., Nittler L. R. and Alexander C. M. O'D. (2014) A titanium oxide grain within a presolar corundum. *Meteorit. Planet. Sci.* 49, Abstract #5389.

Tanaka, H., 2002. Sintering of silicon carbide and theory of sintering. J. Ceram. Soc. Jpn. 110, 877-883.

Tenenbaum, D.D., Dodd, J.L., Milam, S.N., Woolf, N.J., Ziurys, L.M., 2010. Comparative Spectra of Oxygen-rich Versus Carbon-rich Circumstellar Shells: VY Canis Majoris and IRC +10216 at 215-285 GHz, Astrophys. J. 720, L102-L107.

Todini, P., Ferrara, A., 2001. Dust formation in primordial Type II supernovae, Mon. Not. R. Astron. Soc. 325, 726–736.

Travaglio, C., Gallino, R., Amari, S., Zinner, E., Woosley, S., Lewis, R. S., 1999. Low-density graphite grains and mixing in type II supernovae. Astrophys. J., 510, 325–354.

Visscher, C., Lodders, K., Fegley, B., 2006. Atmospheric chemistry in giant planets, brown dwarfs, and low-mass dwarf stars. II. Sulfur and phosphorus. Astrophys. J. 648, 1181-1195.

Vollmer C., Hoppe P., Brenker F.E. and Holzapfel C. (2007) Stellar $MgSiO_3$ perovskite: A shock-transformed stardust silicate found in a meteorite. *Astrophys. J.* 666, L49-L52.

Vollmer, C., Brenker, F. E., Hoppe, P. and Stroud, R. M. (2009) Direct laboratory analysis of silicate stardust from red giant stars. *Astrophys. J.* 700, 774–782.

Lodders, K., & Fegley, B. (2025). Mineral condensation in stellar outflows. In *Presolar Grains in Extra-Terrestrial Materials: Probing Stars with Stardust* (pp. 539-583). Elsevier. https://doi.org/10.1016/B978-0-12-821830-3.00002-4. Revised 29 August 2024. Preprint.

Vollmer, C., Hoppe, P., Stadermann, F.J., Floss, C., Brenker, F.E., 2009. NanoSIMS analysis and Auger electron spectroscopy of silicate and oxide stardust from the carbonaceous chondrite Acfer 094. Geochim. Cosmochim. Acta 73, 7127-7149.

Vollmer C., Hoppe P. and Brenker F.E. (2013) Transmission electron microscopy of Al-rich silicate stardust from asymptotic giant branch stars. *Astrophys. J.* 769:61, (8pp).

Wai, C.M., Wasson, J.T., 1977. Nebular condensation of moderately volatile elements and their abundances in ordinary chondrites. Earth Planet. Sci. Lett. 36, 1-13.

Wai, C.M., Wasson, J.T., 1979. Nebular condensation of Ga, Ge and Sb and the chemical classification of iron meteorites. Nature 282, 790–793.

Wood, J.A., Hashimoto, A., 1993. Mineral equilibrium in fractionated nebular systems. Geochim. Cosmochim. Acta, 57, 2377–2388.

Wiescher, M., Gorres, J., Uberseder, E., Imbriani, G., Pignatari, M., 2010. The Cold and Hot CNO Cycles. Annu. Rev. Nucl. Part. Sci. 60, 381–404.

Wildt, R.W., 1933. Kondensation in Sternatmosphären. Zeit. f. Astrophys. 6, 345-354.

Woosley, S.E., 1997. Neutron-rich Nucleosynthesis in Carbon Deflagration Supernovae. Astrophys. J. 476, 801-810. Doi: 10.1086/303650.

Woosley, S., Heger, A., Weaver, T.A., 2002. Evolution and explosion of massive stars. Rev. Mod. Phys. 74, 1015-1071.

Woosley, S.E., Weaver, T.A., 1995. The evolution and explosion of massive stars. II. Explosive hydrodynamics and nucelosynthesis. Astrophys. J. Suppl. 101, 181-235.

Yoneda, S., Grossman, L., 1995. Condensation of CaO-MgO-Al_2O_3-SiO_2 liquids from cosmic gases. Geochim. Cosmochim. Acta 59, 3413–3444.

Ziurys, L.M., 2006. The chemistry in circumstellar envelopes of evolved stars : Following the origin of the elements to the origin of life. PNAS 103, 12274-12279.

Ziurys, L.M., Schmidt, D.R., Bernal, J.J., 2018. New circumstellar sources of PO and PN: The increasing role of phosphorus chemistry in oxygen-rich Stars, Astrophys. J. 856, id 169 (11pp).